Journal of Applied Mechanics. Received January 16, 2023;
Accepted manuscript posted February 08, 2023. doi:10.1115/1.4056913

Hyperbolicity, Mach lines and super-shear mode III steady state fracture in magneto-flexoelectric materials: II. Crack-tip asymptotics

A.E. Giannakopoulos[1], Ch. Knisovitis[1], Th. Zisis[1], Ares J. Rosakis[2].

[1] Department of Mechanics, School of Applied Mathematical and Physical Sciences, National Technical University of Athens, Athens, Greece

[2] Graduate Aerospace Laboratories, California Institute of Technology, Pasadena, CA, USA.

Corresponding author
A. E. Giannakopoulos,
Email: agiannak@uth.gr

1. Abstract

In our previous study (Part I), the anti-plane steady state hyperbolic mode III fracture of a magneto-flexoelectric material was solved for the displacement, the polarization and the magnetic fields. The solution, however, was based on the assumption of the development of strain discontinuities, and the propagation of the crack-tip was related to a critical shear strain. However, in the current study, the asymptotic details of the fields close to the crack-tip were investigated. The asymptotic analysis assumes strain continuity at the crack-tip (discontinuity in the strain gradients), and reveals the existence of a positive dynamic J-integral. The asymptotic analysis was performed not only for hyperbolic but also for elliptic conditions, and the energy release rate was calculated as a function of the crack-tip velocity in both regimes. These results are very different from those predicted by classical singular elastodynamics, where the dynamic J-integral is zero when super-shear is attained and there can be only an elliptic solution. Moreover, the results are very useful for couple stress elastodynamics where equivalent length scales are present due to the analogy with flexoelectricity.

Keywords: Magneto-flexoelectricity, mode III crack, steady state, asymptotic analysis, energy release rate, couple stress analogy

Journal of Applied Mechanics. Received January 16, 2023;
Accepted manuscript posted February 08, 2023. doi:10.1115/1.4056913

2. Introduction

The flexoelectric effect describes the phenomenon when inhomogeneous strain fields produce polarization in a dielectric material (see Introduction of Part I [1] for a review of the dynamic flexoelectricity literature). This electromechanical property becomes especially important in cases where the mechanical fields are singular. It should be noted that the inverse flexoelectric effect should be included in the energy density formulation [2–4], suggesting that strain gradients will appear when polarization is induced. The mode III fracture regimes considered here could either be sub-shear, which is the only regime possible in classic singular elastodynamics [5,6], or super-shear which has been observed in the context of lattice dynamics [7–9]. The mode III sub-shear asymptotic field of classic elastodynamics can be found in [10]. In this case, the energy flux into the tip of an extending mode III crack in an isotropic elastic solid has been investigated by [11,12]. Incidentally it is interesting to note that flexoelectricity when applied to anti-plane deformations, predicts anti-plane Rayleigh waves [13], and in this context super-shear rupture growth is also super-Rayleigh. In classical elastodynamics anti-plane Rayleigh waves are not possible [14]. Mode III rupture growth at exactly the Rayleigh wave speed corresponds to governing equations that are parabolic.

The Magneto-flexoelectric problem [15] reduces to two uncoupled governing equations, one for the displacement and one for the polarization, with the first one resembling a couple stress elasticity problem [3,13,15–17]. The hyperbolic mode III rupture region has been analyzed in Part I [1] of this study, in which the development of characteristic (Mach) lines for the displacements has been shown. In this part we will provide the crack-tip asymptotic analysis.

In terms of couple stress elasticity, mode III fracture has been studied for the elliptic regime (static and steady state dynamic). Zhang et al. [18] showed that the near tip field is dictated by a single parameter and the validity zone of the asymptotic solution is within a microstructural length. Georgiadis, Gourgiotis, Radi and Tian et al. [19–22] solved the static problem of mode III fracture and calculated the energy release rate.

3. The hyperbolic mode III steady state problem

The anti-plane flexoelectric problem can be described by two parameters, the out-of-plane displacement $u_3(x_1, x_2, t)$ [m] and the out of plane polarization $P_3(x_1, x_2, t)$ [$\mathrm{C\,m^{-2}}$], where x_1, x_2 are the plane coordinates and t is the time. For a flexoelectric material, the energy density can be particularized to the following form (for the general formulation see [2,17,23]), with $(\cdot)_{,i} = \partial(\cdot)/\partial x_i$:

Journal of Applied Mechanics. Received January 16, 2023;
Accepted manuscript posted February 08, 2023. doi:10.1115/1.4056913

$$U=\frac{1}{2}\Big\{aP_3^2+\left(b_{44}+b_{77}\right)\left(P_{3,1}^2+P_{3,2}^2\right)+2e_{44}\left[\left(\varepsilon_{13}+\varepsilon_{31}\right)P_{3,1}+\left(\varepsilon_{23}+\varepsilon_{32}\right)P_{3,2}\right] \\ +2f_{12}\left[\left(\varepsilon_{13,1}+\varepsilon_{31,1}\right)P_3+\left(\varepsilon_{23,2}+\varepsilon_{32,2}\right)P_3\right]+2\mu\left(\varepsilon_{13}^2+\varepsilon_{23}^2\right)\Big\} \tag{1}$$

The materials constants are the density $\rho[\mathrm{kg\,m^{-3}}]$, the atomistic radius $a_0\,[\mathrm{Nm^{-2}}]$, the shear modulus $\mu\,[\mathrm{Nm^{-2}}]$, the flexoelectric constant $f_{12}\,[\mathrm{N\,m\,C^{-1}}]$, the reciprocal dielectric constant $a[\mathrm{N\,m^2\,C^{-2}}]$, the inverse flexoelectric constant $e_{44}\,[\mathrm{N\,m\,C^{-1}}]$, the gradient polarization constant $(b_{44}+b_{77})\,[\mathrm{N\,m^4\,C^{-2}}]$ and $P_{\max}[\mathrm{C/\,m^2}]$ is the polarization strength. Typical values of the constants of some flexoelectric materials are shown in Table 1. In the Following, we briefly present the mechanics of the problem (for details see Part I of this work).

Table 1. Characteristic constants of some flexoelectric materials [16].

Parameter	Dimension	PMMA	$PbTiO_3$	NaCℓ
a_0	nm	–	0.415	0.281
ρ	$\mathrm{kg/\,m^3}$	1180	7520	2160
$c_{44}=\mu$	GPa	2.215	110	12.8
a	$10^8\ \mathrm{Nm^2/\,C^2}$	627.5	0.168	174
$b_{44}+b_{77}$	$10^{-9}\ \mathrm{Nm^4/\,C^2}$	1807	0.115	0.688
$e_{44}-f_{12}$	$\mathrm{Nm/\,C=V}$	7.015	2.00	−2.42
$P_{\max}$	$\mu\mathrm{C/\,cm^2}$	–	57	–
c_s	m/ s	3191	4583	2469
$H/\sqrt{12}$	nm	5.36	2.62	0.199
$\ell/\sqrt{2}$	nm	5.33	2.17	0.113
$H/\left(\ell\sqrt{6}\right)$		1.01	1.21	1.76

Considering an equivalent "microstructural length", an equivalent "micro-inertial length" (as shown in eq. (2) and (3));

$$\frac{\ell^2}{2}=\frac{b_{44}+b_{77}}{a}-\frac{\left(e_{44}-f_{12}\right)^2}{\mu\alpha}\geq 0 \tag{2}$$

$$\frac{H^2}{12}=\frac{b_{44}+b_{77}}{a}\geq\frac{\ell^2}{2} \tag{3}$$

absence of body forces and zero initial electric field, the problem decouples into two equations, one for the polarization (which was studied in previous work) and one for the displacement, eq. (4), which will be used in the current work.

Journal of Applied Mechanics. Received January 16, 2023;
Accepted manuscript posted February 08, 2023. doi:10.1115/1.4056913

$$\mu \nabla^2 u_3 - \mu \frac{\ell^2}{2} \nabla^4 u_3 = \rho \ddot{u}_3 - \frac{\rho H^2}{12} \nabla^2 \ddot{u}_3 \tag{4}$$

The displacement equation (4), which is produced by the decoupling of the problem, must then be modified to accommodate the steady state mode III fracture problem, which is described in Figure 1. In this problem, the crack-tip, propagates in a direction with constant velocity. To capture the movement of the crack-tip, the following steady state transformation should be applied to equation (4).

$$\xi = x_1 + Vt \tag{5}$$

$$\eta = x_2 \tag{6}$$

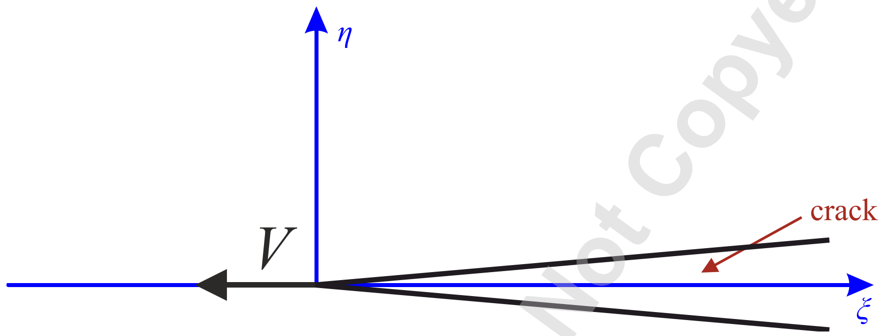

Figure 1. The motion of the steady state mode III fracture with rupture velocity V .

The displacement equation is then transformed to the steady state displacement equation:

$$\left(1-\frac{V^2}{c_s^2}\right)\frac{\partial^2 u_3}{\partial \xi^2} + \frac{\partial^2 u_3}{\partial \eta^2} - \frac{\ell^2}{2}\left(1-\frac{V^2 H^2}{6\ell^2 c_s^2}\right)\frac{\partial^4 u_3}{\partial \xi^4} - \frac{\ell^2}{2}\left(2-\frac{V^2 H^2}{6\ell^2 c_s^2}\right)\frac{\partial^4 u_3}{\partial \xi^2 \partial \eta^2} - \frac{\ell^2}{2}\frac{\partial^4 u_3}{\partial \eta^4} = 0 \tag{7}$$

In the steady state displacement equation, the categorization in Figure 2 can be implemented. The motion could be super-shear if $V > \sqrt{\mu/\rho} = c_s$, or sub-shear if $V < c_s$, elliptic if $(V^2 H^2)/(6\ell^2 c_s^2) < 1$ or hyperbolic if not. The elliptic problem has been solved by [13], while the hyperbolic problem has been presented in Part I of this work. Similar results have been found by [24] in the context of couple-stress elasticity. The hyperbolic problem, which has been solved with the use of the Analogue Equation Method in a finite element code and analytically with the method of the characteristics (Part I), suggests the development of Mach cones with slope:

$$\sin\theta_0 = \sqrt{\frac{1}{\bar{a}^2+1}} \qquad \text{and} \qquad \bar{a} = \sqrt{\frac{H^2 V^2}{6\ell^2 c_s^2} - 1} > 0 \tag{8}$$

Journal of Applied Mechanics. Received January 16, 2023;
Accepted manuscript posted February 08, 2023. doi:10.1115/1.4056913

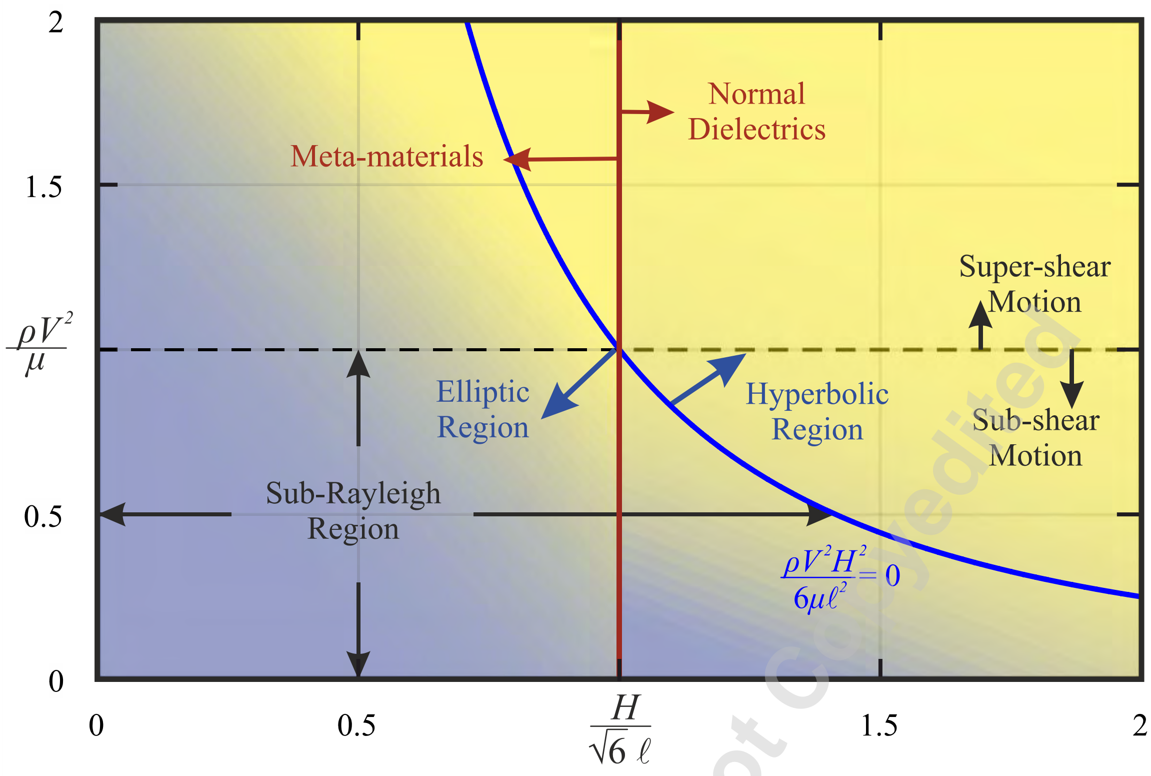

Figure 2. The three regions in which the steady state mode III fracture could reside. Note that a hyperbolic problem could occur for both super-shear and sub-shear crack-tip rapture [1].

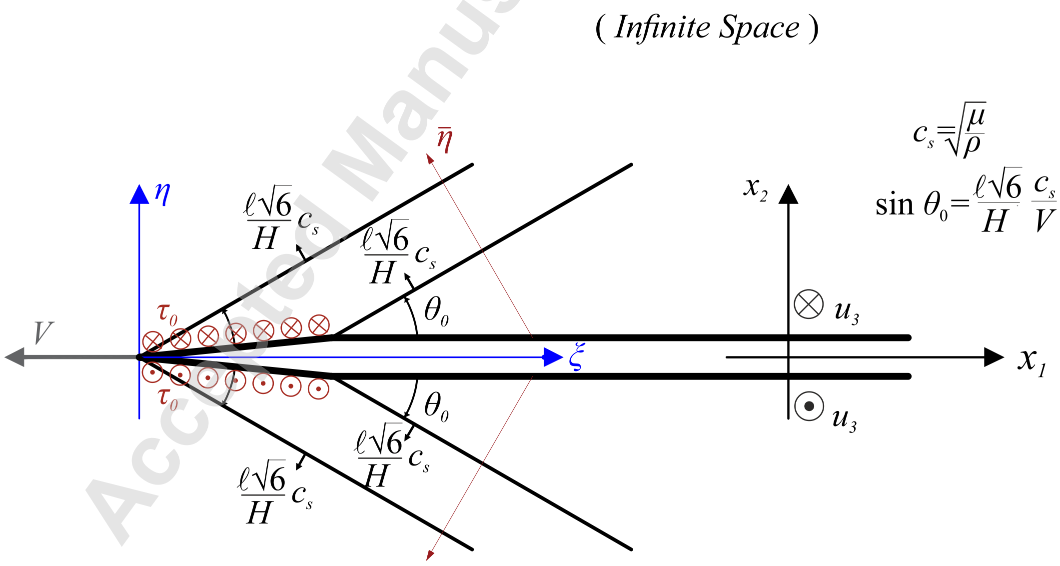

Figure 3. The mode III fracture problem [25] that was solved with the method of the characteristics and the Analogue Equation Method with Finite Elements (see similar Figure 1 of Part I).

Journal of Applied Mechanics. Received January 16, 2023;
Accepted manuscript posted February 08, 2023. doi:10.1115/1.4056913

We particularized our problem to the one suggested by McClintock and Sukhatme [25] for the classic sub-shear case, as shown in Figure 3. The method of characteristics predicts (Part I) the displacement at the end of the loading region $(\xi = L)$ equal to:

$$u_L = \frac{\tau_0 L}{\bar{a}\,\mu} \tag{9}$$

We can assume that this result requires for the propagation of the crack-tip a critical shear strain:

$$\gamma_c = \frac{\tau_0}{\bar{\alpha}\mu} \tag{10}$$

Note that inside the elliptic region, if bounded by the velocity $V / c_s \leq 1$, there is a sub-Rayleigh region as found by [13].

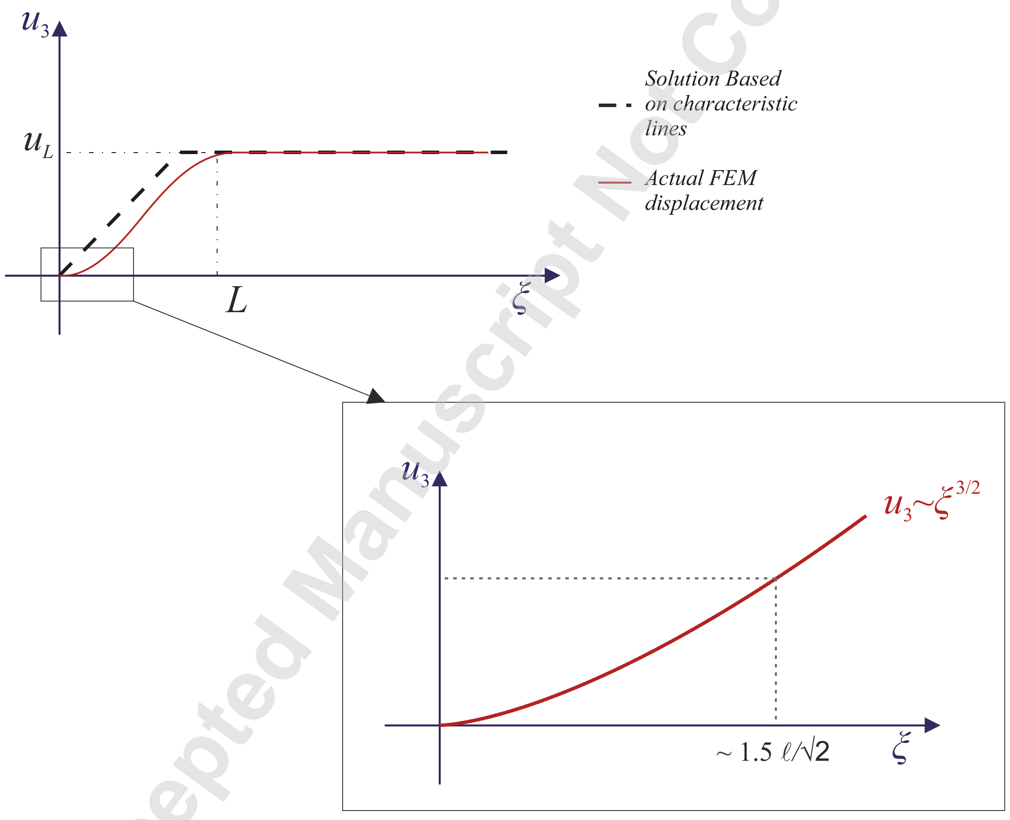

Figure 4. The displacement suggested by the solution based on the characteristics with strain discontinuity at the crack-tip and at the end of the loading region and by the solution given by the Analogue Equation Method with Finite Elements (Part I). Strain continuity leads to a cusp-like displacement examined in this work.

Journal of Applied Mechanics. Received January 16, 2023;
Accepted manuscript posted February 08, 2023. doi:10.1115/1.4056913

4. Asymptotic solution near the crack-tip

Assuming strain continuity, we consider the possibility of a cusp-type asymptotic displacement, in the vicinity near the crack-tip $(r \to 0)$, in terms of polar coordinates $r^2 = \xi^2 + \eta^2$, $\tan\theta = \eta/\xi$, attached to the moving crack-tip (Figure 4). Recent experimental work on dynamic Mode II rupture suggests such cusp-type displacement [26]. Conjecturing from the static and the sub-Rayleigh dynamic cases, we assume that the leading term of the asymptotic which can provide positive energy release is:

$$u_3 = \mathrm{O}\left(r^{3/2}\right) \tag{11}$$

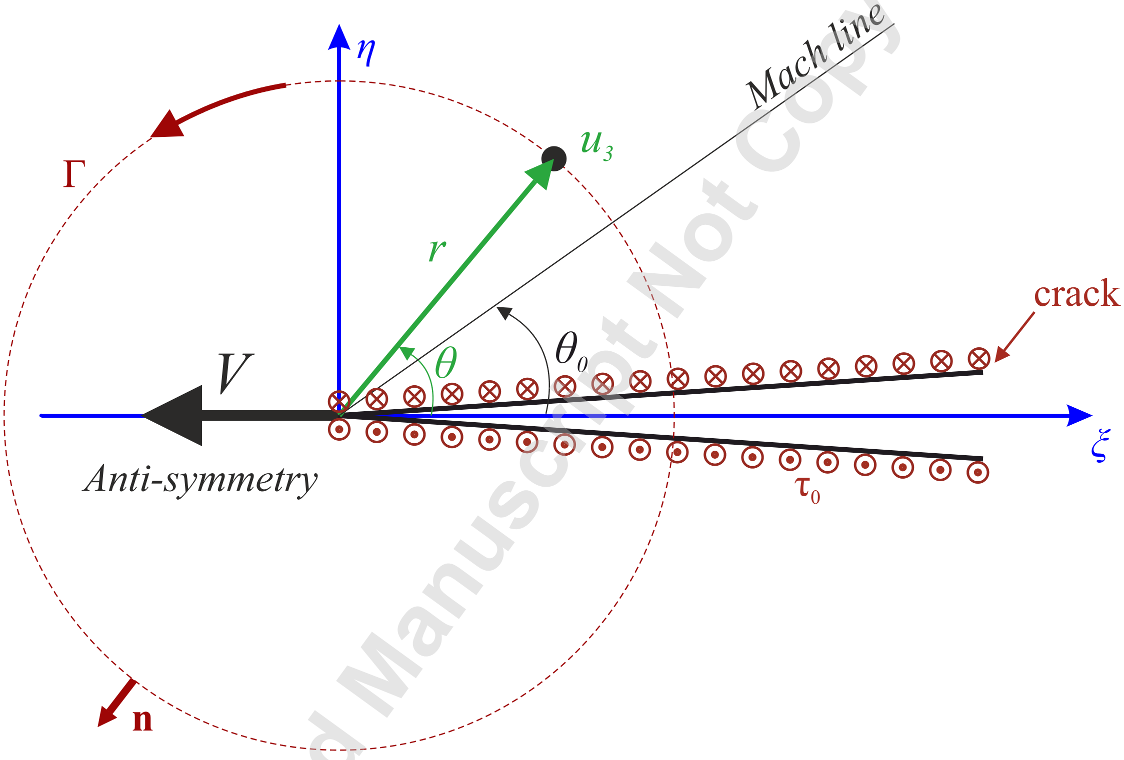

Figure 5. Polar coordinates used in the asymptotic analysis and the circular contour Γ used for the evaluation of the J-integral, where u_3 is antisymmetric with respect to ξ coordinate. Note that $L \gg \ell/\sqrt{2}$.

It is tacitly assumed that the motion of the crack-tip is determined in terms of a specific surface fracture energy (Griffith-like fracture criterion), as envisaged by [27] for a mode II crack. Such asymptotic relation can provide a positive energy release rate at the crack-tip. This asymptotic displacement should obey the following differential equation, which contain only the highest derivatives of the equilibrium equation (7), with $\nabla^2 = \partial^2/\partial\xi^2 + \partial^2/\partial\eta^2$:

Journal of Applied Mechanics. Received January 16, 2023;
Accepted manuscript posted February 08, 2023. doi:10.1115/1.4056913

$$\nabla^4 u_3 - \lambda\, \nabla^2 u_{3,\xi\xi} \approx 0, \quad \lambda = \frac{H^2 V^2}{6\ell^2 c_s^2} > 0 \tag{12}$$

It will be later confirmed from Finite Element Method (FEM) results that the leading asymptotic term takes the form:

$$u_3 = u_3\left(r,\, \theta;\, \lambda\right) \approx r^{3/2}\, F\left(\theta;\, \lambda\right) \tag{13}$$

By substituting (13) to (12) we obtain the differential equation for $F(\theta;\lambda)$:

$$\begin{aligned} 4\left(1-\lambda\sin^2\theta\right)F^{IV} - 12\,\lambda\sin\theta\cos\theta\, F^{\mathrm{III}} + \left(4\,\lambda\cos^2\theta - 7\,\lambda + 10\right)F^{\mathrm{II}} \\ -27\,\lambda\sin\theta\cos\theta F^{\mathrm{I}} - \left(\frac{45}{4}\lambda\cos^2\theta - \frac{18}{4}\lambda - \frac{9}{4}\right)F = 0 \end{aligned} \tag{14}$$

$(F^I = \partial F / \partial\theta,\, F^{II} = \partial^2 F / \partial\theta^2,\, F^{III} = \partial^3 F \partial\theta^3,\, F^{IV} = \partial^4 F / \partial\theta^4)$.

The general solution of (14) takes the form;

$$\begin{aligned} F\left(\theta;\, \lambda\right) = c_1\left(\lambda\right)\sqrt{1-\cos\theta}\left(2\cos\theta+1\right) + c_2\left(\lambda\right)\sqrt{1+\cos\theta}\left(2\cos\theta-1\right) + \\ c_3\left(\lambda\right)\cos\left[\frac{3}{2}\arcsin\left(\frac{\cos\theta}{\sqrt{1-\lambda\sin^2\theta 1}}\right)\right]\left(1-\lambda\sin^2\theta\right)^{3/4} + \\ c_4\left(\lambda\right)\,\Big(\sqrt{\sin\theta\sqrt{1-\lambda}+\cos\theta\sqrt{-1}}\,\sin\theta\sqrt{1-\lambda} \\ +\sqrt{\sin\theta\sqrt{1-\lambda}+\cos\theta\sqrt{-1}}\,\cos\theta\sqrt{-1} \\ -\sqrt{\sin\theta\sqrt{1-\lambda}-\cos\theta\sqrt{-1}}\,\sin\theta\sqrt{1-\lambda} \\ +\sqrt{\sin\theta\sqrt{1-\lambda}-\cos\theta\sqrt{-1}}\,\cos\theta\sqrt{-1}\Big) \end{aligned} \tag{15}$$

where $c_i(\lambda) = 1,2,3,4$ are (complex) constants that depend on λ and on the boundary conditions. Note that $\lambda = \overline{a}^2 + 1 = (H^2V^2)/(6\ell^2 c_s^2)$ and that for the static case $\lambda = 0$. We will examine the region $0 \le \theta \le \pi$, noting that $F(\theta) = F(-\theta)$ for $-\pi \le \theta \le 0$.

Regarding the boundary condition along the crack face, $(\theta = 0)$, we assume vanishing couple stress traction:

$$\frac{\partial^2 u_3}{\partial \eta^2} = 0 \tag{16}$$

and vanishing stress traction:

Journal of Applied Mechanics. Received January 16, 2023;
Accepted manuscript posted February 08, 2023. doi:10.1115/1.4056913

$$\frac{\partial u_3}{\partial \eta} - \frac{\ell^2}{2}\frac{\partial}{\partial \eta}\left[\frac{\partial^2 u_3}{\partial \xi^2} + \frac{\partial^2 u_3}{\partial \eta^2} + (1-\lambda)\frac{\partial^2 u_3}{\partial \xi^2}\right] = 0 \tag{17}$$

Asymptotically $(r \to 0)$ these boundary conditions reduce to:

$$\begin{aligned} &\left(\frac{1}{r}\frac{\partial}{\partial r} + \frac{1}{r^2}\frac{\partial^2}{\partial \theta^2}\right)u_3\bigg|_{\theta=0} = 0 \\ &\nabla^2 u_{3,\eta} + (1-\lambda)u_{3,\eta\xi\xi}\Big|_{\theta=0} = 0 \end{aligned} \tag{18}$$

4.1. Asymptotes for the Elliptic case

The asymptotic results for the elliptic case ($0 \le \lambda = (H^2V^2)/(6\ell^2 c_s^2) < 1$) can be found from eq.(15) with B.C. (18) along the crack face and

$$\begin{aligned} &F(\pi;\, \lambda) = 0 \\ &\left(\frac{1}{r}\frac{\partial}{\partial r} + \frac{1}{r}\frac{\partial}{\partial \theta}\right)F(\theta;\, \lambda)\bigg|_{\theta=\pi} = 0 \end{aligned} \tag{19}$$

in front of the crack tip ($\theta = \pi$). As a result, we obtain;

$$\begin{aligned} F(\theta;\, \lambda) = \bar{B}_{ellp}\Bigg\{ &\frac{4(\lambda-1)}{3\lambda}\left[(2\cos\theta+1)\sqrt{1-\cos\theta} + (\lambda-2)\left(\cos\theta - \frac{1}{2}\right)\sqrt{1+\cos\theta}\right] \\ &-\frac{2(\lambda-4)}{3\lambda}\cos\left[\left(\frac{3}{2}\right)\arcsin\left(\frac{\cos\theta}{\sqrt{\lambda\cos^2\theta - \lambda + 1}}\right)\right]\left(\lambda\cos^2\theta - \lambda + 1\right)^{3/4} \\ &-\sqrt{2\sqrt{\lambda\cos^2\theta - \lambda + 1} + 2\sin\theta\sqrt{1-\lambda}}\,\cos\theta \Bigg\} \end{aligned} \tag{20}$$

where the constant;

$$\bar{B}_{ellp} = \bar{B}_{ellp}(\lambda) = \bar{B}\,\frac{3\sqrt{2}}{4(\lambda-4)} \tag{21}$$

And $\bar{B}$ is the amplitude of the asymptotic solution (to be determined by the full solution of the problem):

Journal of Applied Mechanics. Received January 16, 2023;
Accepted manuscript posted February 08, 2023. doi:10.1115/1.4056913

$$\bar{B} = \lim_{r\to 0} \frac{u_3(r,\theta=0)}{r^{3/2}} = F(\theta=0;\lambda) \tag{22}$$

For the static case $\lambda \to 0$, the solution returns to the static solution that was proposed by [18,19] and the particular solution proposed by [21].

$$\lim_{\lambda\to 0} F(\theta;\lambda) = \bar{B}_{static}\left[3\cos\left(\frac{\theta}{2}\right)+5\cos\left(\frac{3\theta}{2}\right)\right] = \bar{B}\left[\frac{3}{8}\cos\left(\frac{\theta}{2}\right)+\frac{5}{8}\cos\left(\frac{3\theta}{2}\right)\right] \tag{23}$$

Note that $\bar{B} = 8\,\bar{B}_{static} = -16\,(\bar{B}_{ellp}(\lambda=1))\,/\,(3\sqrt{2})$. For $\lambda \to 1$, it can be seen that for angles greater than $\pi/2$ the displacement is zero, as will be confirmed from the solution of the hyperbolic problem. The normalized angle variation of the asymptotic displacement is shown in Figure 6 for a range of normalized rupture velocities $\sqrt{\lambda} < 1$. Note that as $\sqrt{\lambda} \to 1$ (the Rayleigh wave speed) $u_3 \approx 0$ for $\pi/2 \le \theta \le \pi$, i.e. in front of the crack-tip, and so a vertical Mach line at $\theta = \pi/2$ will emerge and will carry over to the hyperbolic (post-Rayleigh rupture) regime $\sqrt{\lambda} > 1$ (see later Figure 9).

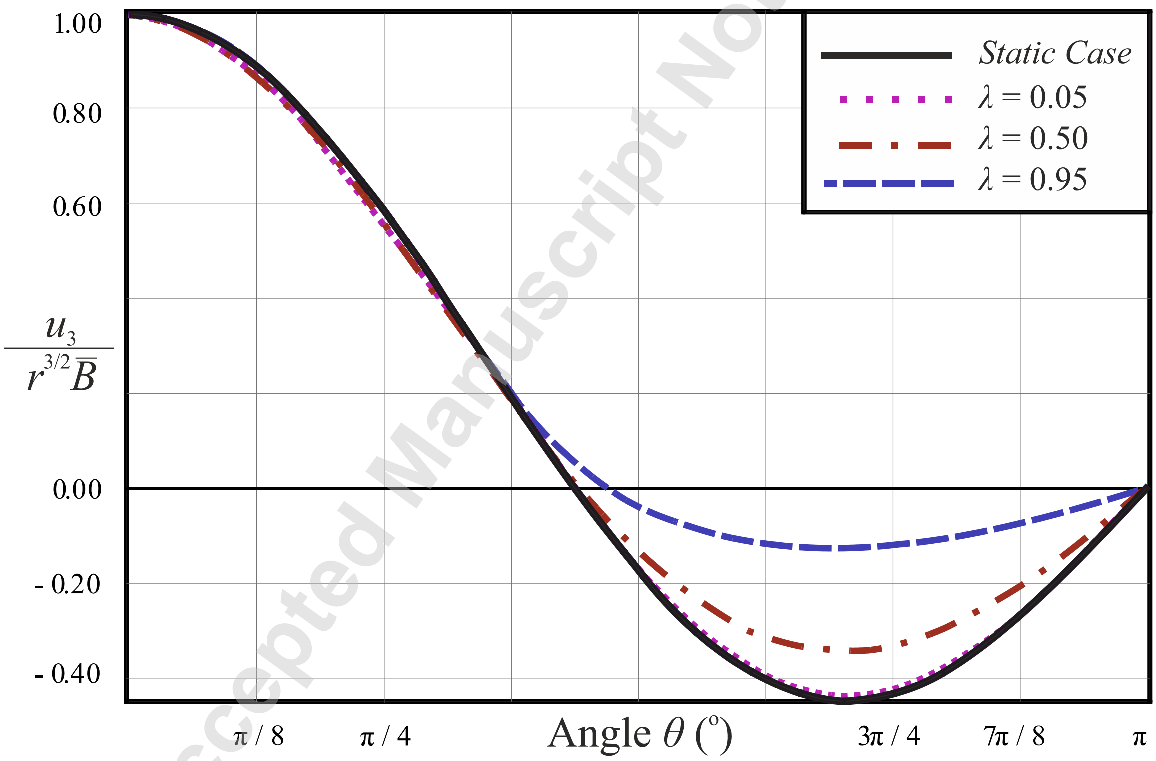

Figure 6. Angle variation of the normalized asymptotic displacement for the elliptic anti-plane steady state problem, for a range of λ.

A short account for the classic elastodynamics elliptic case ($0 \le V / c_s \le 1$) is given in Appendix A.

Journal of Applied Mechanics. Received January 16, 2023;
Accepted manuscript posted February 08, 2023. doi:10.1115/1.4056913

4.2. Asymptotes for the Hyperbolic case

For the hyperbolic case $(\lambda > 1)$, finite element results focusing close to the crack-tip (see later Figure 11) reveal three regions as shown in Figure 7. The FEM results suggest an additional boundary should be considered vertical to the crack:

$$u_3\Big|_{\theta=\pi/2} = 0 \tag{24}$$

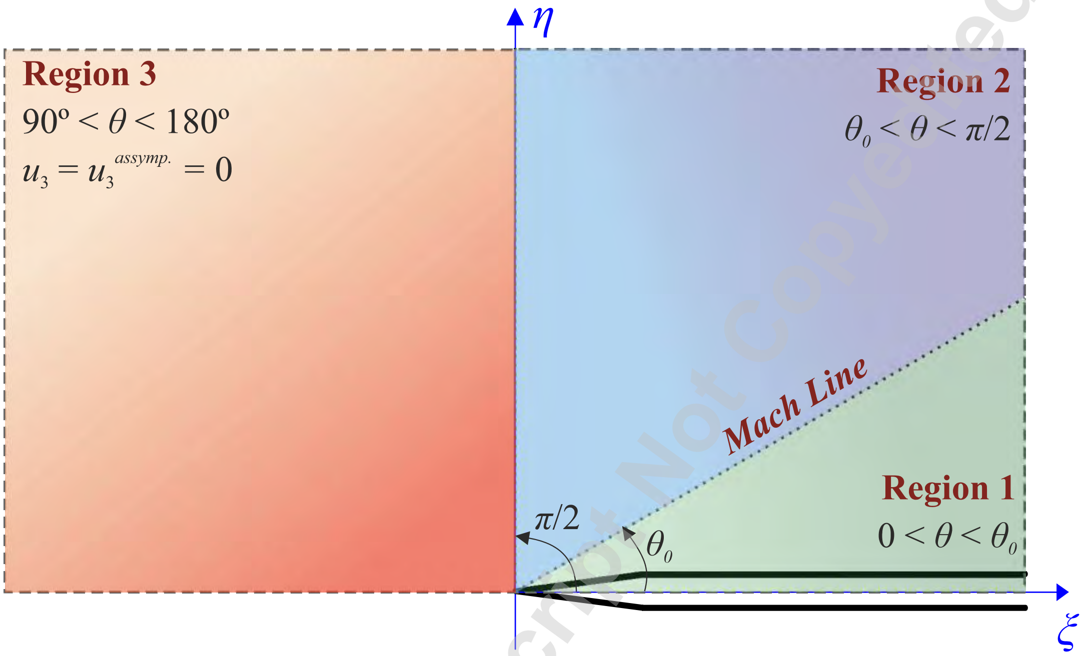

Figure 7. The 3 different regions that appear asymptotically close to the crack-tip $(\sin\theta_0 = 1/\sqrt{\lambda})$ that are also suggested by FEM solution.

Therefore, for region 3, $\pi/2 \le \theta \le \pi$ in front of the crack-tip, we have $u_3 = 0$.

For region 2, $\theta_0 \le \theta \le \pi/2$, where $\sin\theta_0 = 1/\sqrt{\lambda}$ (characteristic line) the analytic solution for $F(\theta)$ is:

$$F(\theta;\, \lambda) = \bar{A}_2 \left(\sin\frac{3\theta}{2} + \cos\frac{3\theta}{2} \right) \tag{25}$$

while in the last region 1 the analytic solution takes the following form

Journal of Applied Mechanics. Received January 16, 2023;
Accepted manuscript posted February 08, 2023. doi:10.1115/1.4056913

$$F(\theta;\,\lambda)=\bar{A}_1\Big[\big(\cos\theta-\sin\theta\sqrt{\lambda-1}\big)\sqrt{\left|\cos\theta-\sin\theta\sqrt{\lambda-1}\right|}$$
$$+\big(\cos\theta+\sin\theta\sqrt{\lambda-1}\big)\sqrt{\left|\cos\theta+\sin\theta\sqrt{\lambda-1}\right|} \tag{26}$$
$$+\sqrt{2}\,(\lambda-1)(2\cos\theta-1)\sqrt{1+\cos\theta}\Big]$$

The displacement continuity at $\theta=\theta_0$ suggests that $\bar{A}_2$, $\bar{A}_1$ and $\bar{B}$ are connected through the following relation.

$$\bar{A}_2=\frac{\bar{B}\sqrt{2}}{\lambda}\frac{\left[(\lambda-1)\sqrt{\lambda-1}-0.5\lambda^{3/2}+0.5\sqrt{\lambda}\right]\sqrt{\sqrt{\lambda}+\sqrt{\lambda-1}}+(\lambda-1)^{3/4}}{\lambda^{3/4}\left\{\sin\left[3\arcsin\left(1/\sqrt{\lambda}\right)/2\right]+\cos\left[3\arcsin\left(1/\sqrt{\lambda}\right)/2\right]\right\}} \tag{27a}$$

$$\bar{A}_1=\bar{B}\,\frac{1}{2\lambda} \tag{27b}$$

Finite element analysis supports eq. (25) and (26), as can be shown in Figure 8.

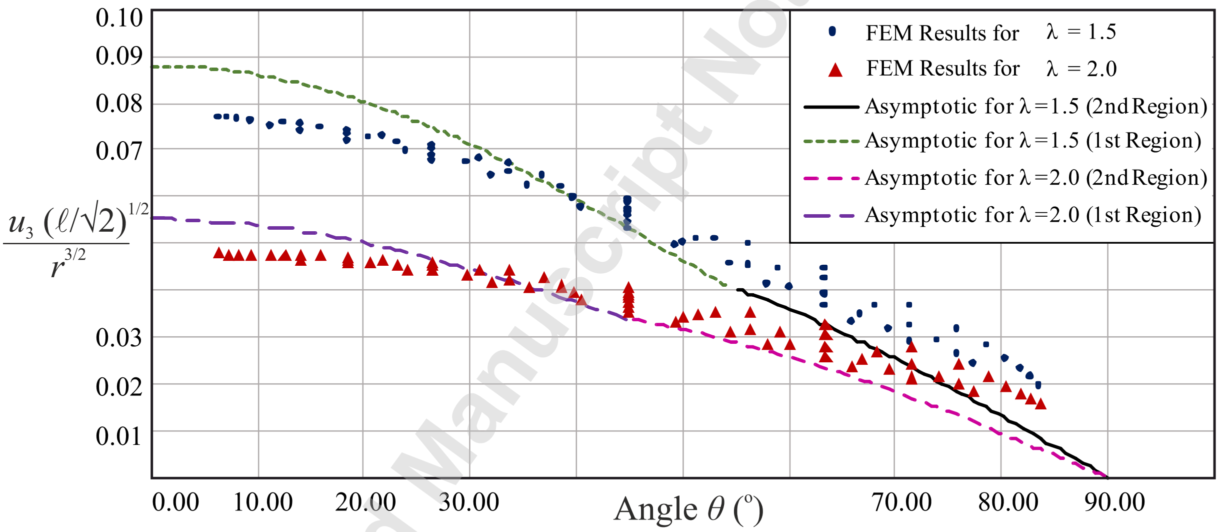

Figure 8. The asymptotic solution for $\lambda=1.50$, $\lambda=2.00$, according to the FEM code, and the theoretical approach for region of validity $(2/3)\,\ell/\sqrt{2}$ and $\tau_0/\mu=4.00\ 10^{-2}$.

A special case can be considered for $\lambda=1$. The angular variation of the displacement can be given as follows.

$$F(\theta;\lambda)\approx 2\,\bar{A}_1\,(\cos\theta)^{3/2} \tag{28}$$

Finite element analysis supports eq. (28), as can be shown in Figure 9. However, in this case $\bar{A}_1\to\infty$.

Journal of Applied Mechanics. Received January 16, 2023;
Accepted manuscript posted February 08, 2023. doi:10.1115/1.4056913

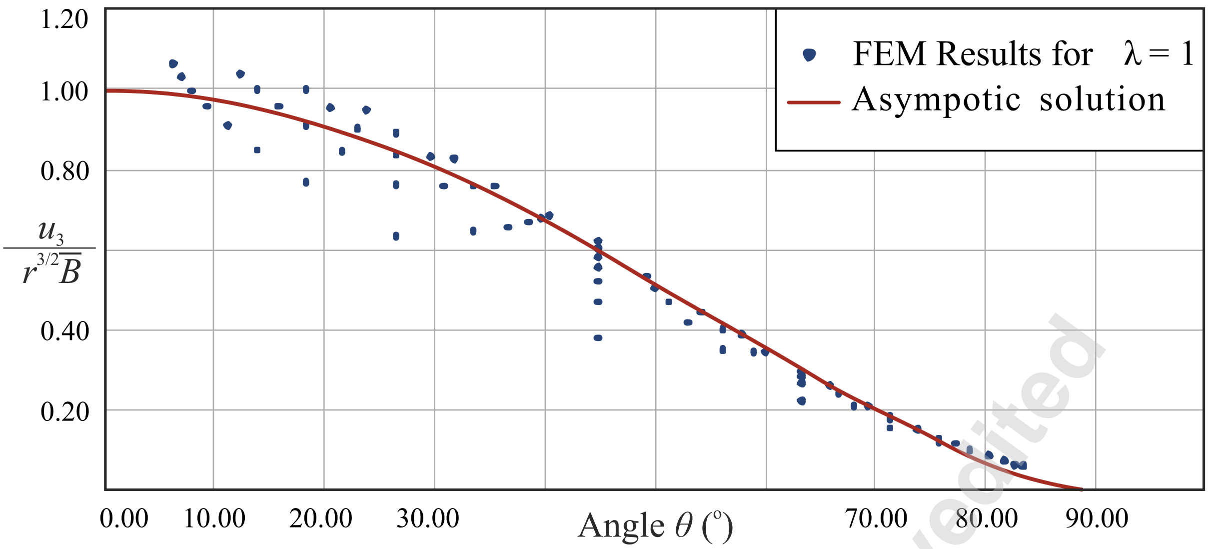

Figure 9. The asymptotic solution for $\lambda = 1.00$ according to the FEM and its theoretical estimate (28) for $\tau_0 / \mu = 4.00\ 10^{-2}$.

The region on validity of the asymptotic order $O(r^{3/2})$ is for $r < \xi_1 = (3/2)(\ell/\sqrt{2})$. However, the solution of the characteristic lines begins from a point further away as $\tan\varphi \neq (3/2)\xi_1^{1/2}\overline{B} = [\partial u_3^{asym} / \partial r]_{r=\xi_1}$. From the FEM results (Figure 10), the normalized asymptotic amplitude $\overline{B}$ can be approximated as:

$$\left(\frac{\ell}{\sqrt{2}}\right)^{1/2} \overline{B} \approx \frac{\tau_0}{\mu} \frac{1}{\sqrt{\lambda - 1}} \tag{29}$$

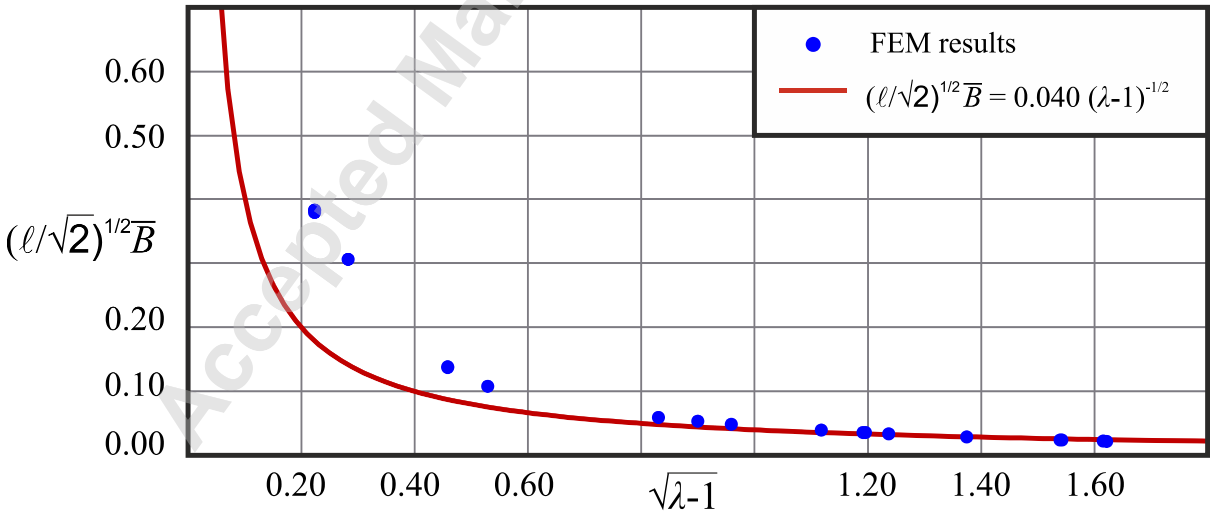

Figure 10. The numeric values of the parameter $\overline{B}$ in the hyperbolic problem according to the results close to the crack-tip finite element analysis, for $\tau_0 / \mu = 4.00\ 10^{-2}$.

Journal of Applied Mechanics. Received January 16, 2023;
Accepted manuscript posted February 08, 2023. doi:10.1115/1.4056913

The solution for the displacement u_3 may include terms of greater order (see for example [28] for the plate analogue asymptotics). For example, taking the next term in the asymptotic solution we have:

$$u_3 = \bar{B}\ r^{3/2} + \bar{C}\ r^2 \tag{30}$$

This solution holds for $\xi_1 \le r \le \xi_2$, where ξ_2 is the point where characteristic line solution becomes dominant. Assuming that for ξ_1 there is displacement continuity between the near and the far field;

$$\bar{C} = \frac{\bar{B}}{\xi_1} = \left(\frac{3}{2}\frac{\ell}{\sqrt{2}}\right)^{-1/2} \bar{B} \tag{31}$$

and that at $\xi_2 = \kappa\,\xi_1$ $(\kappa > 1)$, the gradients of the characteristic line and the second term asymptotic are the same:

$$2\bar{C}\xi_2 = \tan\theta_0 \quad \Rightarrow \quad 2\bar{C}\left(\kappa\,\xi_1\right) = \tan\theta_0 \tag{32}$$

Inserting (31) in (32), we obtain:

$$\bar{B}\left(\frac{\ell}{\sqrt{2}}\right)^{1/2} = \kappa^{-1}\frac{\sqrt{2}}{2\sqrt{3}}\tan\theta_0 \tag{33}$$

Acquiring from the FEM solution the result (29), we conclude that for the particular problem:

$$\kappa^{-1}\frac{\sqrt{2}}{2\sqrt{3}}\tan\theta_0 \approx \left(25\,\frac{\tau_0}{\mu}\right)0.073\tan\theta_0 \quad \Rightarrow \quad \kappa = 0.2237\,\frac{\tau_0}{\mu} \tag{34}$$

Thus, near the crack-tip, the characteristic line solution is secondary to the asymptotic behavior, within a radius of

$$0 \le r \le 0.3356\,\frac{\tau_0}{\mu}\,\frac{\ell}{\sqrt{2}} \tag{35}$$

For larger radius, characteristic line solution dominates as can be seen from Figure 11.

Journal of Applied Mechanics. Received January 16, 2023;
Accepted manuscript posted February 08, 2023. doi:10.1115/1.4056913

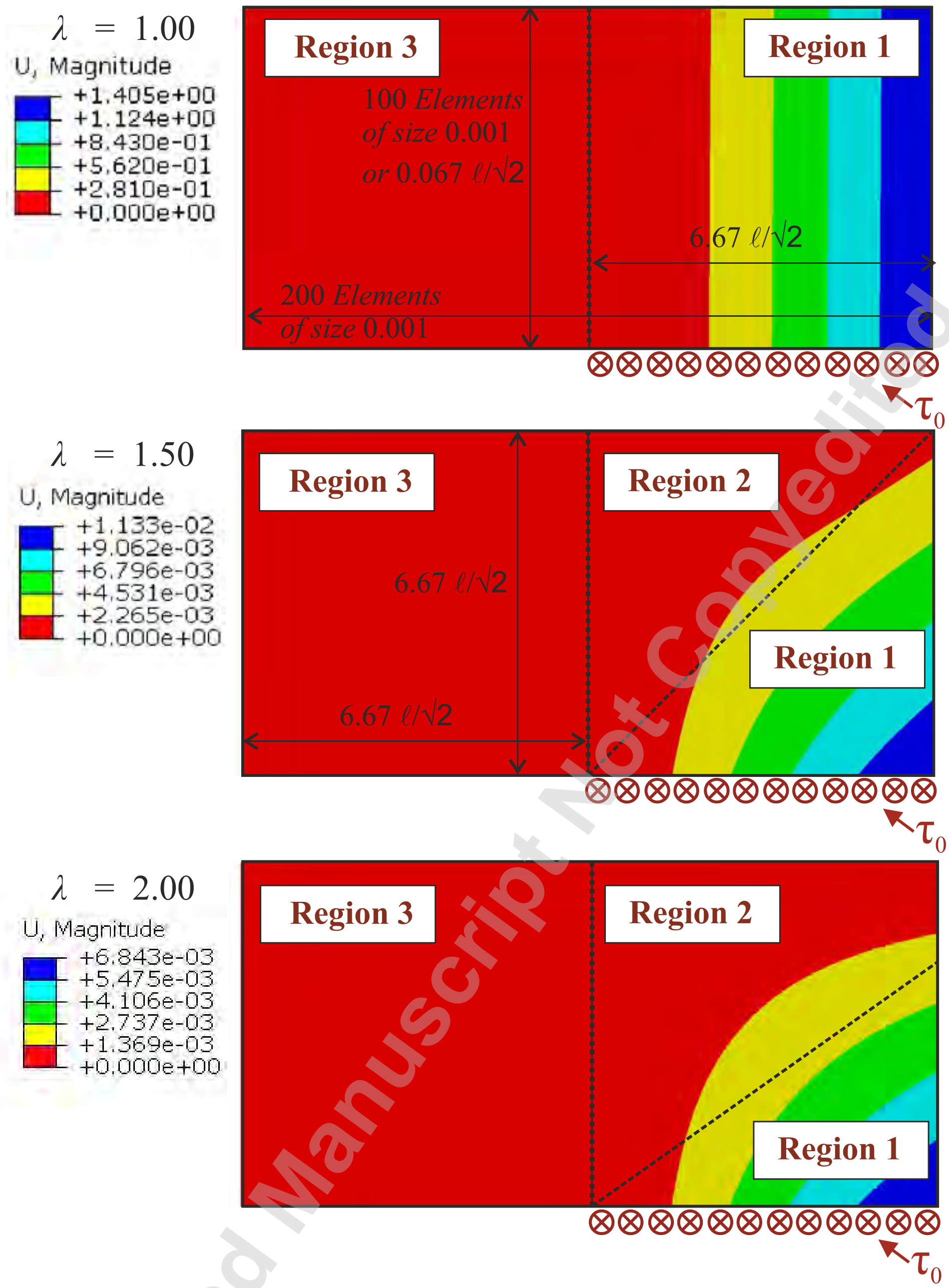

Figure 11. The three regions of the asymptotic solution, as computed by the finite elements (the general purpose code ABAQUS [29] was used), for $\tau_0 / \mu = 4.00\ 10^{-2}$.

Journal of Applied Mechanics. Received January 16, 2023;
Accepted manuscript posted February 08, 2023. doi:10.1115/1.4056913

5. The Energy Release Rate

From the analogy of the present problem with that of the couple stress elasticity we can obtain the dynamic J-integral ($\Im$), introduced by Freund [11]. In the general flexoelectric case, the dynamic J-integral is given in the Appendix of [16]. For the present problem, the J-integral is derived from Appendix B. Considering the form of the displacement described by eq.(13), as $r \to 0$, only the fourth order derivatives in the formulation of the J-integral should not be neglected and thus:

$$\begin{aligned}\Im = 2\int_0^{\pi} \Bigg\{ & \frac{V^2}{2}\left[\rho\, u_{3,x}^2 \cos\theta + \frac{\rho H^2}{12}\left(u_{3,xy}^2 + u_{3,xx}^2\right)\cos\theta \right. \\ & \left. - \frac{\rho H^2}{6} u_{3,x}\left(u_{3,xxx}\cos\theta + u_{3,yxx}\sin\theta\right)\right] \\ & + \frac{\mu}{2}\left[\left(u_{3,y}^2 + u_{3,x}^2\right)\cos\theta - 2\,u_{3,x}\,u_{3,y}\sin\theta\right] + \\ & + \frac{\mu\ell^2}{2}\left[\frac{1}{2}\left(\nabla^2 u_3\right)^2\cos\theta - \nabla^2 u_3\left(u_{3,xx}\cos\theta + u_{3,xy}\sin\theta\right) + \right. \\ & \left. + u_{3,x}\left(\nabla^2 u_{3,x}\cos\theta + \nabla^2 u_{3,y}\sin\theta\right)\right]\Bigg\} r\, d\theta \end{aligned} \tag{36}$$

Equation (36) was derived for a crack rupture in the opposite direction than that of Figure 5. Thus for eq. (36) to be compatible with eqs. (20), (25), (26) the θ argument should be mapped to ($\pi - \theta$). Then, the energy release rate can be simplified for both the Elliptic (sub-Rayleigh) and the hyperbolic (super-Rayleigh) problem as:

$$\begin{aligned}\frac{\Im}{\bar{B}^2 \mu\,\ell^2} = 2\int_0^{\pi} \Bigg\{ & \frac{1}{64}\left(9F + 4F^{II}\right)\left[\left(4F^{II} - 3F\right)\cos\theta + 8F^{I}\sin\theta\right] \\ & + \frac{\lambda}{4}\Bigg\{\left[\left(F^{II}\right)^2 + \frac{9}{2}FF^{II}\right]\cos\theta\sin^2\theta - \left[F^{I}F^{II} + 3FF^{I}\left(\cos^2\theta + \frac{1}{2}\right)\right]\sin\theta \\ & - \left[\left(F^{I}\right)^2\left(\cos^2\theta - \frac{5}{4}\right) + \frac{9}{4}F^2\left(\frac{5}{4}\cos^2\theta - 2\right)\right]\cos\theta\Bigg\}\Bigg\} d\theta \end{aligned} \tag{37}$$

The normalized energy release rate for the elliptic case ($0 \le \lambda < 1$) can be found from eq. (37) by inserting the asymptotic solution found in (20) and the result is shown in Figure 12

Journal of Applied Mechanics. Received January 16, 2023;
Accepted manuscript posted February 08, 2023. doi:10.1115/1.4056913

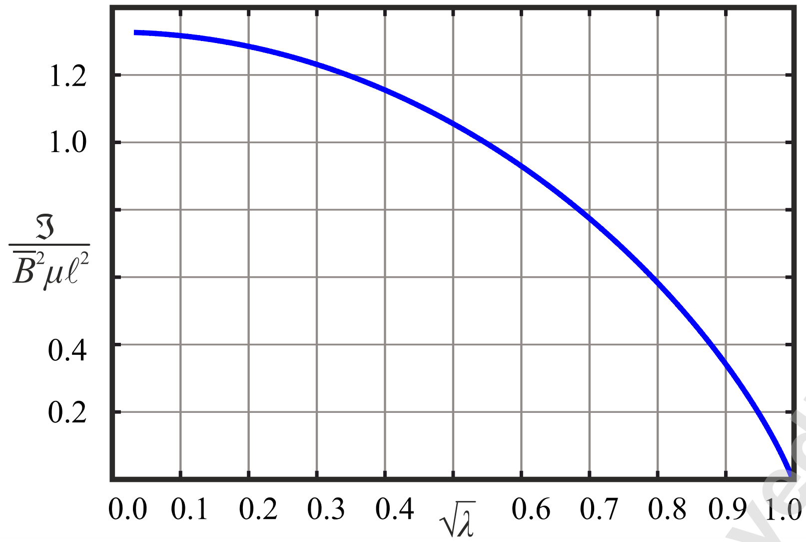

Figure 12. The normalized energy release rate for the elliptic (sub-Rayleigh) case $(0 \le \lambda < 1)$.

For the static case ($\lambda \to 0$), we obtain:

$$\Im_{static} = 1.325\,\bar{B}^2\mu\ell^2 \tag{38}$$

in accord with [18,19,21].

For the hyperbolic case ($\lambda > 1$) the energy release rate can be found by eq. (37) using the asymptotic solution found in eq. (25) and (26). The normalized result for the energy release rate can be depicted in Figure 13. For $\lambda \to 1$, its normalized value is zero[*], while as $\lambda \to \infty$ the normalized energy release rate tends to infinity. Note that a positive energy flux into the rupture front is possible in the entire hyperbolic (super-Rayleigh) regime, as found for a mode II crack propagation with a velocity weakening and with a rate-dependent cohesive zone by [30,31].

[*] Note that the zero normalized value of the J-integral does not make the J-integral itself zero. The parameter $\bar{B}$ may take an infinite value, rendering the J-integral infinite. On the other hand, other types of loading could result in $J = 0$ at $\sqrt{\lambda} = 1$, see for example [27].

Journal of Applied Mechanics. Received January 16, 2023;
Accepted manuscript posted February 08, 2023. doi:10.1115/1.4056913

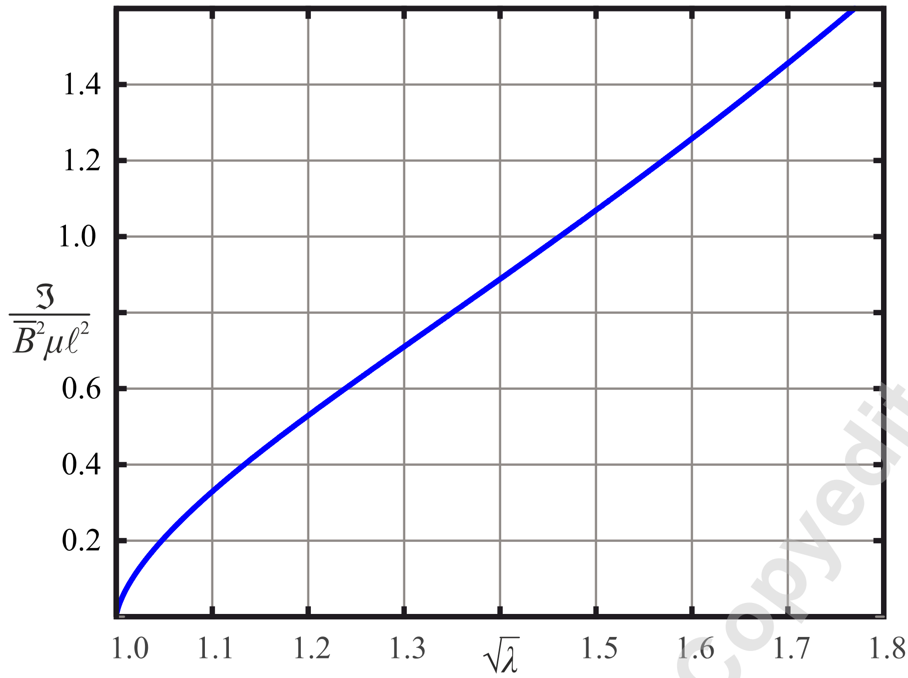

Figure 13. The normalized energy release rate for the hyperbolic mode III steady state crack $\lambda = (H^2V^2)/(6\ell^2 c_s^2)$.

Figure 14 shows the normalized energy release rate for both the sub-Rayleigh $(0 \le \lambda < 1)$ and the super-Rayleigh $(\lambda > 1)$ cases. For $\lambda = 1$, both the elliptic and the hyperbolic cases give:

$$\frac{\Im}{\overline{B}^2\mu\ell^2} = 0; \ \sqrt{\lambda} = 1 \tag{39}$$

Journal of Applied Mechanics. Received January 16, 2023;
Accepted manuscript posted February 08, 2023. doi:10.1115/1.4056913

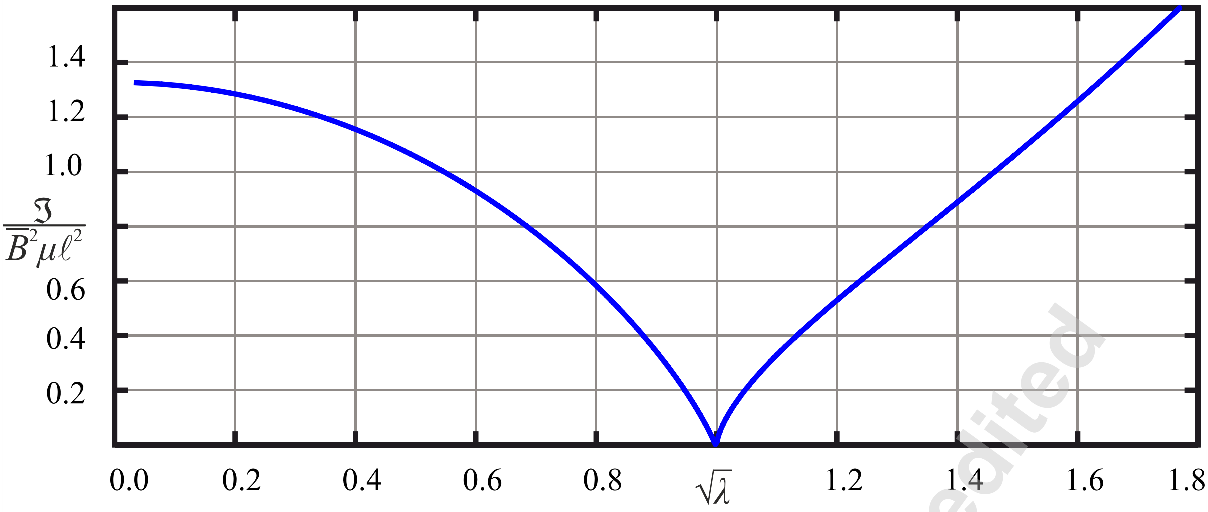

Figure 14. The normalized energy release rate for the anti-plane mode III fracture in a flexoelectric material.

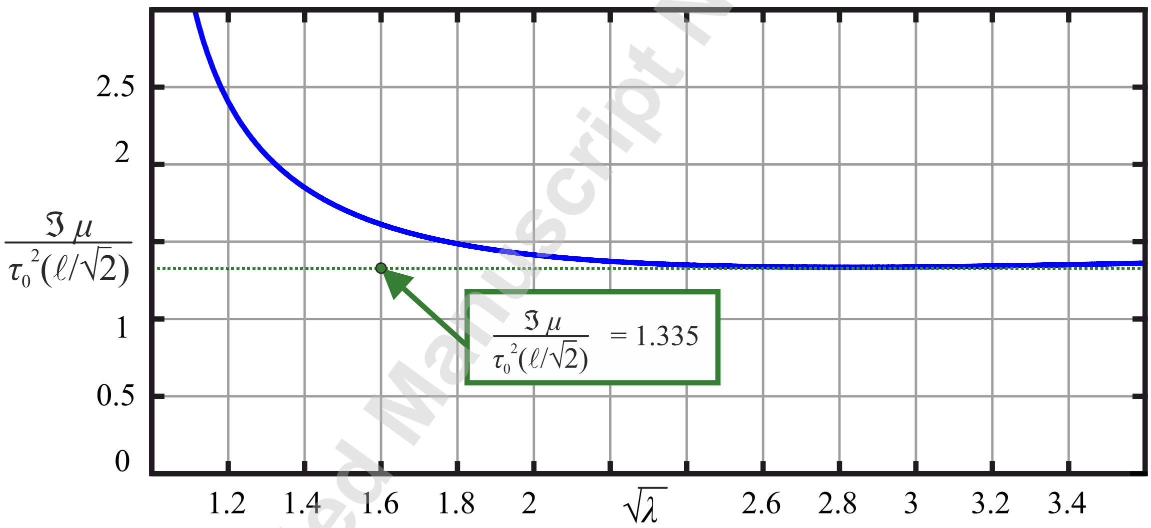

Figure 15. The normalized energy release rate for the particular loading and $\lambda > 1$. Note that for this problem $\bar{B}$ can be given from eq. (29).

To complete the evaluation of the J-integral we need the asymptotic amplitude $\bar{B} = u_3(r,\theta=0)/r^{3/2}$, which can be estimated from FE (eq. (29)). Figure 13 $(\lambda > 1)$ can be combined with eq. (29) and the energy release rate can be renormalized as in Figure 15.

In addition, we can normalize the J-integral (found form FEM) with its static value and obtain Figure 16. Note that the J-integral for the static case has been estimated by [16] as:

Journal of Applied Mechanics. Received January 16, 2023;
Accepted manuscript posted February 08, 2023. doi:10.1115/1.4056913

$$\Im_{static} \approx \frac{4\tau_0^2 L}{\pi \mu}\left(1-e^{-\frac{L}{3\ell}}\right) \tag{40}$$

Equation (40) implies a shielding effect due to the microstructural length ℓ. For $\ell = 0$, eq. (40) gives the classic static value of $(4\tau_0^2 L)/(\pi\mu)$.

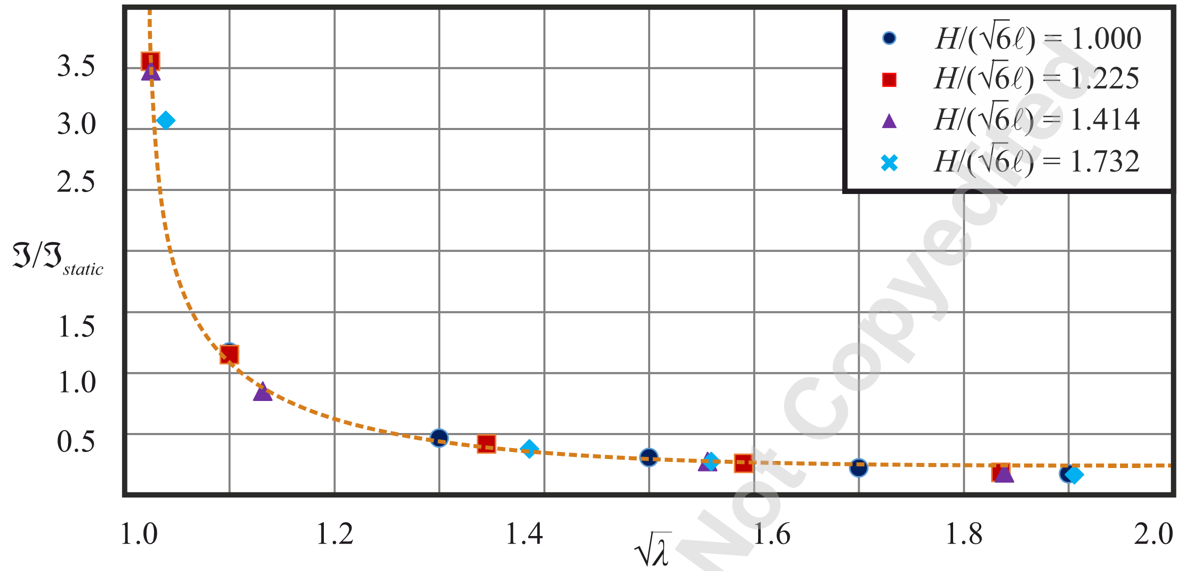

Figure 16. The normalized J-integral with respect to the static case, where the results show the combined influence of V/c_s and $H/(\sqrt{6}\ell)$ in the parameter $\sqrt{\lambda} = (HV)/(\sqrt{6}\ell c_s)$ for $\tau_0/\mu = 4.00\ 10^{-2}$, and $L/(\ell/\sqrt{2}) = 6.667$.

A good approximation for $\lambda < 1$ was given by [16] as:

$$\frac{\Im}{\Im_{static}} \approx \frac{1}{\sqrt{1-\lambda}} \tag{41}$$

Considering a Griffith like fracture criterion, rupture occurs when the energy release rate is equal to a critical value, unique for each material. The critical energy release rate $\Im_{critical}$ that starts the crack tip motion ($\lambda > 0$) occurs for a critical shear stress $\tau_{critical}$:

$$\Im_{critical} = \frac{4\tau_{critical}^2 L}{\pi \mu} \tag{42}$$

This criterion is equivalent to critical slip displacement. For the elliptic case ($\lambda < 1$):

$$\frac{|\tau_0|}{\tau_{critical}} \approx \left[\frac{\sqrt{1-\lambda}}{1-e^{-L/(3\ell)}}\right]^{1/2} \tag{43}$$

Journal of Applied Mechanics. Received January 16, 2023;
Accepted manuscript posted February 08, 2023. doi:10.1115/1.4056913

For the hyperbolic case ($\lambda > 1$), the energy release rate can be given by $\Im = \tau_0^2(\ell/\sqrt{2})Q(\lambda)/\mu$, with $Q(\lambda)$ the dimensionless quantity obtained by Figure 15. Demanding the energy release rate to be equal with its critical value, the normalized shear loading $\tau_0/\tau_{critical}$ can be given by the following relation:

$$\frac{|\tau_0|}{\tau_{critical}} \approx \left[\frac{4}{\pi}\frac{L}{\ell}\frac{1}{\sqrt{2}}\frac{1}{Q(\lambda)}\right]^{1/2} \tag{44}$$

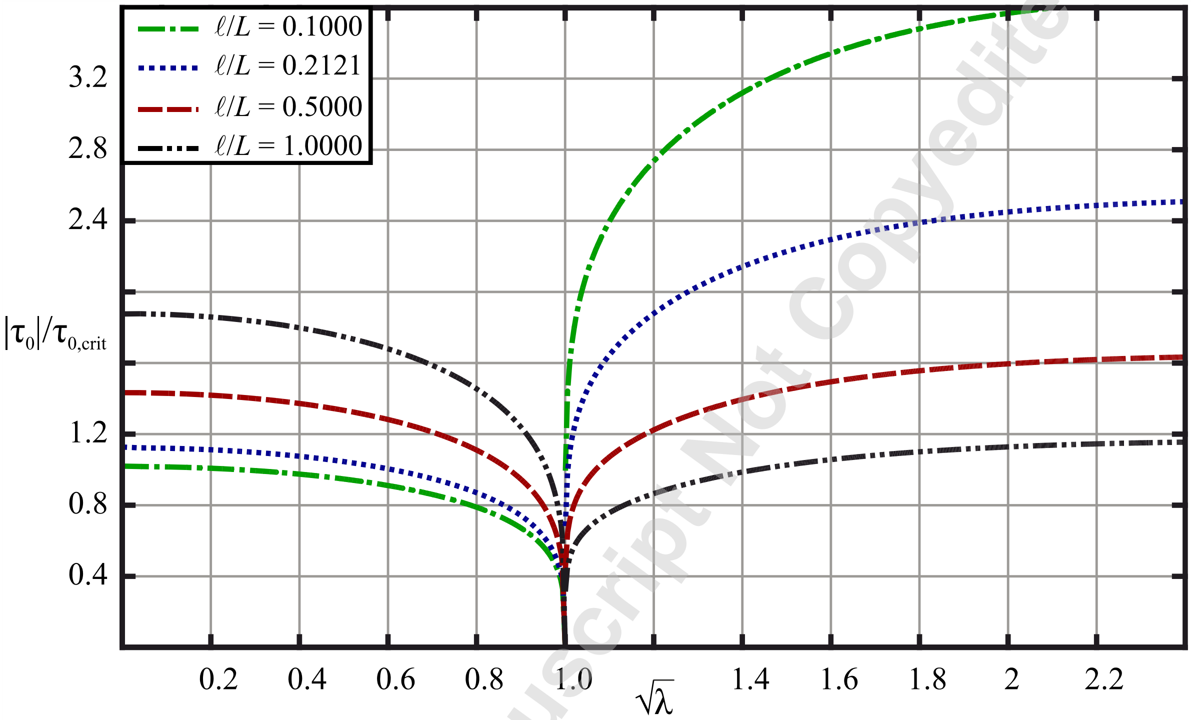

Figure 17. The approximate normalized shear stress with respect to the critical shear, for which crack starts to propagate. For a specific shear stress, crack tip accelerates and it is possible to jump to super-shear rupture.

Note that for $\sqrt{\lambda} < 1$ the strength increases with ℓ/L showing a size dependency. For $\sqrt{\lambda} > 1$ and $\ell \to 0$, the super-Rayleigh region cannot be reached, as predicted by classic elastodynamics.

Journal of Applied Mechanics. Received January 16, 2023;
Accepted manuscript posted February 08, 2023. doi:10.1115/1.4056913

6. Burridge-Andrews type of dynamic crack advance

The previous analysis implies that, if the crack-tip can attain super-Rayleigh velocities $(\sqrt{\lambda} > 1)$, then there can be a steady state admissible crack tip velocity $\sqrt{\lambda} \geq 2$. This velocity limit is independent of the loading and can be viewed as a critical normalized rupture velocity. A similar result has been found theoretically and experimentally for mode II fracture under slip-weakening friction with admissible rupture velocity in the intersonic range; $c_s\sqrt{2} \leq V \leq c_d$, where $c_s = \sqrt{\mu / \rho}$ is the shear wave velocity and c_d is the dilatation velocity (see for example [32–34]). However, the lack of transient solutions for our problem precludes us at this point to investigate the conditions governing the transition from sub-Rayleigh velocities to super-Rayleigh velocities. Regarding mode III classic elastodynamics, Andrews [33] proposed a slip-weakening interface model that removes the stress singularity, creating a cohesive zone in front of the crack-tip. The same slip-weakening interface model has been utilized by [35] who investigated the nucleation of mode III rupture and its transition to crack-like self-similar rupture in the context of classic elastodynamics. They found that super-sonic speed is allowed after a time that scales with the nucleation time. Dunham [36] presented a very thorough analysis on the conditions governing the occurrence of super-shear ruptures under Dugdale type slip-weakening friction. He proposed that ruptures jump between sub-Rayleigh and intersonic speeds when fast moving stress waves of the rupture reach the peak strength of the fault and initiate slip in the form of a "daughter" crack ahead of the main crack, as Burridge [37] initially suggested for self-similar crack models. An emerging super-shear "daughter" mode II crack propagating at a characteristic velocity $\sqrt{2}\,c_s$ has been experimentally observed by [38] and numerically for a crack with a velocity weakening cohesive zone by [30]. In this work we predict that the crack-tip asymptotic displacement in the moving with the tip coordinate system varies as $(\xi^2 + \eta^2)^{3/4}$, as found by [39] for slip - weakening rupture instability. An overview of the analysis of super-shear mode III transition in rupture experiments that includes the effect of nucleation condition and friction parameters is given in [40].

Moreover, our previous analysis [13] implies that for a sub-Rayleigh solution, a local maximum shear traction appears ahead of the main crack-tip, as the Burridge scenario implies;

$$t_{\max} \simeq 0.585 \frac{K_{III}}{\sqrt{2\pi}} \ell^{-1/2} \sqrt{\frac{\rho_1}{\rho_2}}, \qquad K_{III} = \frac{2\tau_0\sqrt{2\pi L}}{\pi}, \qquad \rho_1 = 1 - \frac{V^2}{c_s^2}, \qquad \rho_2 = 1 - \frac{H^2 V^2}{6\ell^2 c_s^2} \quad (45)$$

which increases with V / c_s up to a critical shear strength that will make the crack jump to the intersonic range. This maximum shear stress occurs at a distance;

$$\xi_{\max} \approx 1.3\,\ell \sqrt{\frac{\rho_1}{\rho_2}} \leq 1.3\,\ell \quad (46)$$

which decreases with V / c_s and approaches the major crack. The zero-shear stress occurs at a distance;

Journal of Applied Mechanics. Received January 16, 2023;
Accepted manuscript posted February 08, 2023. doi:10.1115/1.4056913

$$\xi_0 \approx 0.43\ \ell \sqrt{\frac{\rho_1}{\rho_2}} \leq 0.43\ \ell \tag{47}$$

which also decreases with V / c_s. These results are implying that a "daughter" crack, could appear at a certain load level and could move towards the major crack. Our model does not need a slip weakening cohesive zone [41,42] in order to trigger the "daughter" crack scenario [43], because it includes an a-priori length scale which results to a local maximum traction in front of the major crack. Further analysis on the transient problem can be very useful for the study of fast ruptures and the "mother – daughter" crack interaction.

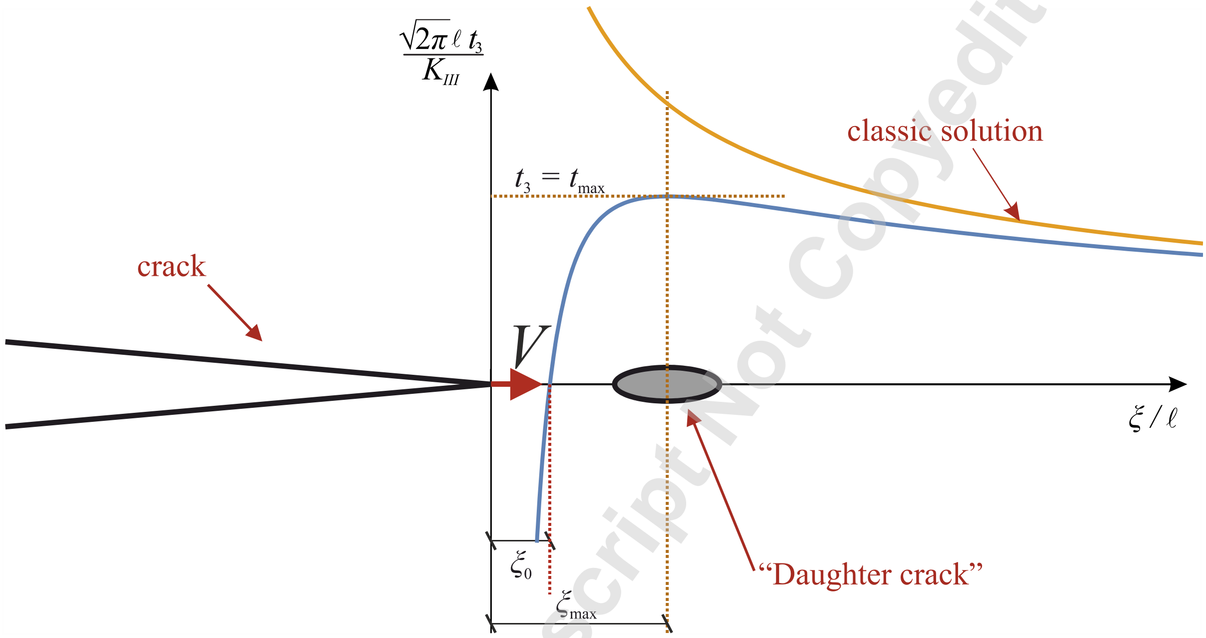

Figure 18. Schematic of a Burridge – Andrews type of dynamic crack advance based on [13]. Note that the classic solution holds outside our present solution.

7. Conclusion

This work examines the near crack-tip structure of the dynamic steady state mode III fracture in flexoelectric materials propagating along a weak crack path line. The asymptotic near field displacement was estimated within the elliptic, parabolic and hyperbolic regimes which are all possible withing the context of flexoelectricity. It was shown that the asymptotic displacement near the crack-tip is of order $O(r^{3/2})$, that is a cusp-type spatial variation and thus ensures uniqueness for the solution. For the limit of "small" rupture speeds the asymptotic near field displacement agrees with the available solutions in the literature. For rupture speeds approach the Rayleigh wave speed the elliptic regime prediction reduced to the expected parabolic predictions. The displacement field for the hyperbolic regime is found to be composed of three

Journal of Applied Mechanics. Received January 16, 2023;
Accepted manuscript posted February 08, 2023. doi:10.1115/1.4056913

independent regions while the amplitude of the asymptotic displacements depends on a common parameter, which is estimated using finite element results. In the limit of the rapture tip to the Rayleigh wave speed from above, the parabolic point is also approached.

Lastly, the dynamic J-integral was calculated for all type of conditions as a function of the normalized rupture velocity $\sqrt{\lambda} = (H^2V^2)/(6\ell^2 c_s^2)$. For static conditions ($\lambda = 0$), the J-integral agreed with the literature, for the parabolic condition ($\lambda = 1$) it was found to be singular, while for the elliptic ($\lambda < 1$) and the hyperbolic ($\lambda > 1$) regimes was always positive.

These results can also be useful for couple and dipolar stress elastodynamics due to the shown analogy with flexoelectricity. The results are sharply different to those of classic mode III elastodynamics that do not predict Rayleigh waves and feature zero dynamic J-integral at super-shear rapture velocities.

Appendix A. The classic Elliptic (sub-shear) case

The classic sub-shear case for mode III fracture was studied by Freund [44]. The displacement near the crack-tip ($r \to 0$) can be described as (in accord with Figure 5);

$$u_3 = \frac{2K_{III} r^{1/2}}{\mu\sqrt{2\pi}a_s}\left\{1 - \left[\frac{V\sin(\pi-\theta)}{c_s}\right]^2\right\}^{1/4} \sin\frac{\theta_s}{2} \tag{A.1}$$

with:

$$a_s = \sqrt{1-\left(\frac{V}{c_s}\right)^2} \qquad \tan\theta_s = a_s \tan(\pi-\theta) \tag{A.2}$$

For the static case ($V/c_s \to 0$), (A.1) is reduced to;

$$\lim_{V/c_s \to 0}\left(u_3 \frac{a_s \mu\sqrt{2\pi}}{2K_{III} r^{1/2}}\right) = \cos\frac{\theta}{2} \tag{A.3}$$

while for $V/c_s \to 1$, the displacement is being described as;

$$\frac{u_3 \mu a_s \sqrt{2\pi}}{2K_{III} r^{1/2}} = \begin{cases} (\cos\theta)^{1/2}, & 0 \le \theta \le \dfrac{\pi}{2} \\ 0, & \dfrac{\pi}{2} \le \theta \le \pi \end{cases} \tag{A.4}$$

Journal of Applied Mechanics. Received January 16, 2023;
Accepted manuscript posted February 08, 2023. doi:10.1115/1.4056913

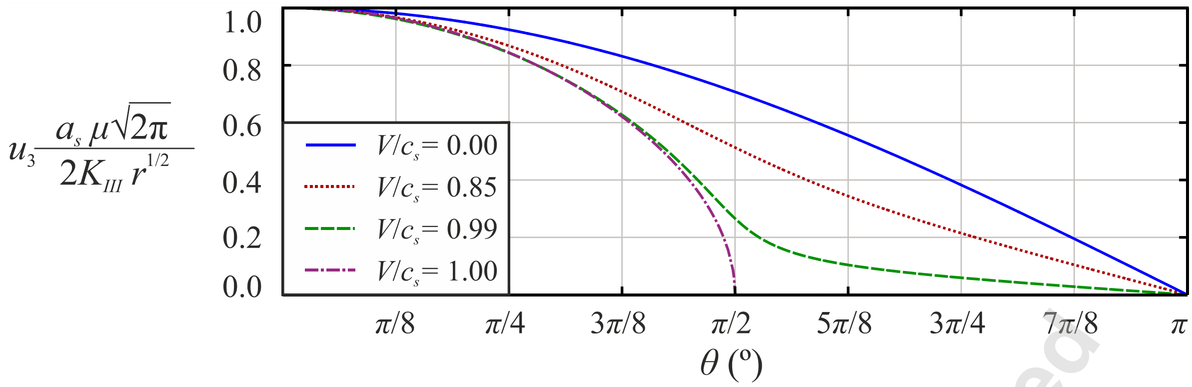

Figure A.1. The Normalized mode III classic elastodynamic displacement (considering the parameter a_s) A region with zero displacement appears as the velocity reaches the limiting velocity V/c_s.

The Energy Release Rate (J-integral) can be given as:

$$\Im = \frac{K_{III}^2}{2\mu\sqrt{1-\left(\frac{V}{c_s}\right)^2}} \tag{A.5}$$

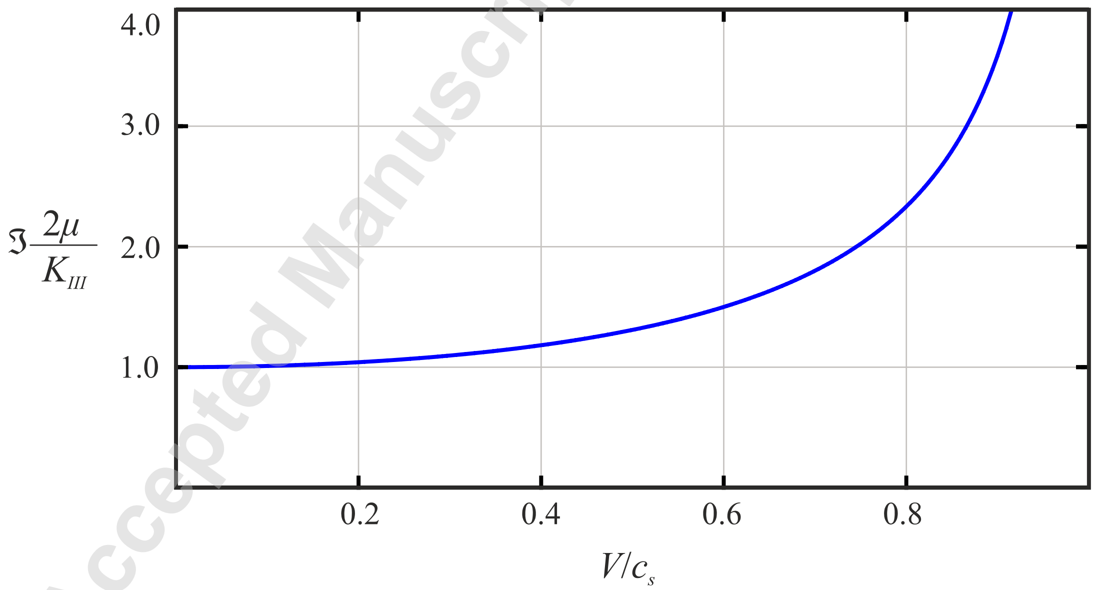

Figure A.2. The mode III J-Integral for the classic elastodynamics (sub-shear) case

Journal of Applied Mechanics. Received January 16, 2023;
Accepted manuscript posted February 08, 2023. doi:10.1115/1.4056913

Appendix B. The uniqueness of the elastodynamics solution of the running crack in mode III rupture of flexoelectrics

The uniqueness of the solution for the classic static case was shown through the boundness of u_3 [45]. The standard uniqueness theorem in classic linear elastodynamics with appropriate boundary conditions was stated in [46]. An extension of the proof to include unbounded domains was presented by [47]. For the static gradient and couple elasticity [48] we obtain the following continuity relations:

- R_0 is the domain R without the crack faces $(\xi \le 0, \eta = \pm 0)$
- R^+ is the domain R above the ξ axis without the crack-tip $(n \ge 0, \xi \ne 0)$
- R^- is the domain R below the ξ axis without the crack-tip $(n \le 0, \xi \ne 0)$
- Smoothness condition of the displacement and its derivatives:

$$\begin{aligned}
&u_3 \in C^1\left(D^+\right) \cap C^1\left(D^-\right) \cap C^4\left(D_0\right) \\
&\left\{\frac{\partial u_3}{\partial x_1}, \frac{\partial u_3}{\partial x_2}\right\} \in C\left(D^+\right) \cap C\left(D^-\right) \cap C^3\left(D_0\right) \\
&\left\{\frac{\partial^2 u_3}{\partial x_1^2}, \frac{\partial^2 u_3}{\partial x_1 \partial x_2}, \frac{\partial^2 u_3}{\partial x_2^2}\right\} \in C\left(D^+\right) \cap C\left(D^-\right) \cap C^2\left(D_0\right)
\end{aligned} \tag{B.1}$$

- Necessary edge conditions for the field near the crack tip that guarantees unique solution [48]:

$$u_3, \frac{\partial u_3}{\partial x_1}, \frac{\partial u_3}{\partial x_2} : \text{must be bounded} \tag{B.2}$$

For running cracks, the classic elastodynamics uniqueness was shown by Freund and Clifton [49] for crack tip speed less than the Rayleigh wave speed of the material.

To prove the uniqueness of the elastodynamics solution for the running crack in mode III rupture of flexoelectrics, we will follow the work of Freund and Clifton [49]. We start from the equilibrium equation in absence of body forces (4), multiply it by $\dot{u}_3$ and then, integrate it in any region R around the crack tip:

$$I = \int_R \left(\mu \nabla^2 u_3 - \mu \frac{\ell^2}{2} \nabla^4 u_3 - \rho \ddot{u}_3 + \frac{\rho H^2}{12} \nabla^2 \ddot{u}_3 \right) \dot{u}_3 da = 0 \tag{B.3}$$

Let υ_n be the velocity of any point on curve S_1, that encircles the crack-tip, in the normal direction on $\vec{n}$, as shown in Figure B.1. The region R is between the outer boundary S, the inner curve S_1 and the crack faces.

Journal of Applied Mechanics. Received January 16, 2023;
Accepted manuscript posted February 08, 2023. doi:10.1115/1.4056913

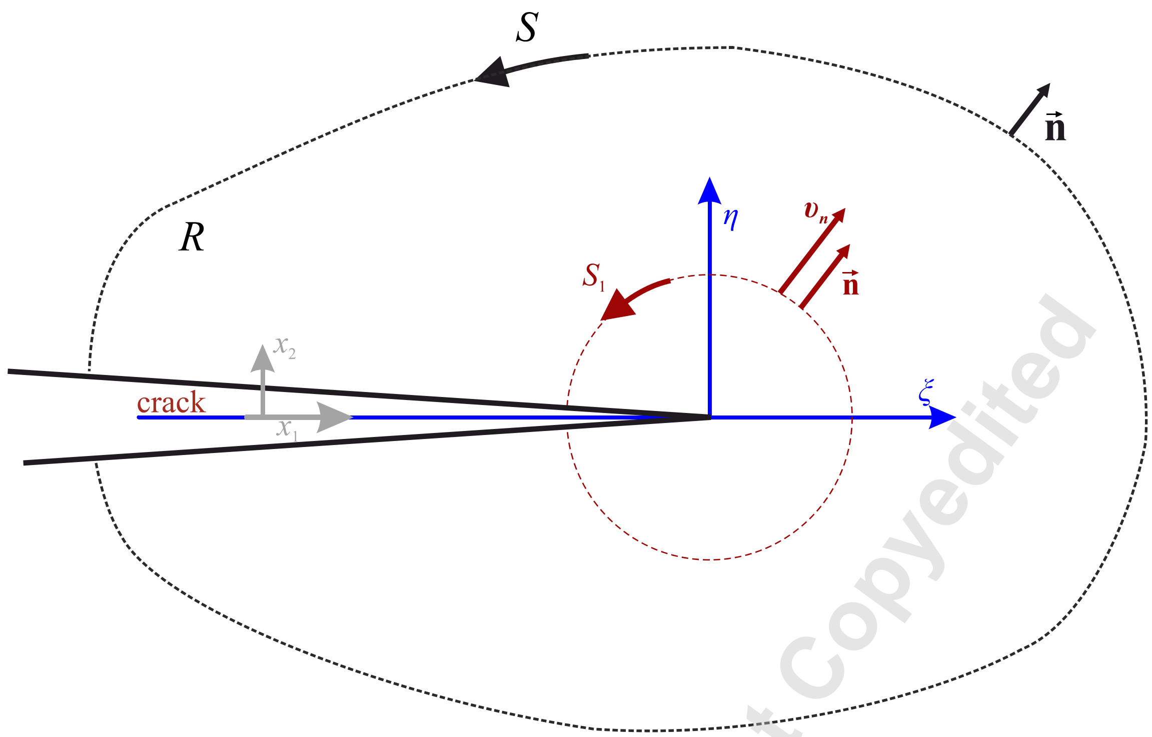

Figure B.1. The crack tip configurations at a certain time instant. (x_1, x_2) is the fixed coordinate system and (ξ, η) is the coordinate system moving with the crack-tip.

Equation (B.3) can be modified by expanding each term and then it can be rewritten as:

Journal of Applied Mechanics. Received January 16, 2023;
Accepted manuscript posted February 08, 2023. doi:10.1115/1.4056913

$$
\begin{aligned}
I = & \iint_{S_1}\left[\mu\vec{\nabla}u_3\dot{u}_3-\mu\frac{\ell^2}{2}\vec{\nabla}\left(\nabla^2u_3\right)\dot{u}_3\right]\cdot\vec{n}ds \\
& +\frac{d}{dt}\iint_{R}\left(-\mu\vec{\nabla}u_3\cdot\vec{\nabla}u_3-\mu\frac{\ell^2}{2}\nabla^2u_3\nabla^2u_3\right)da+\frac{d}{dt}\int_{S_1}\mu\frac{\ell^2}{2}\left(\nabla^2u_3\vec{\nabla}u_3\right)\cdot\vec{n}ds \\
& +\int_{S_1}\mu\vec{\nabla}u_3\cdot\vec{\nabla}u_3\upsilon_n ds+\int_{S_1}-\mu\frac{\ell^2}{2}\vec{\nabla}\cdot\left(\nabla^2u_3\vec{\nabla}u_3\right)\upsilon_n ds+\int_{S_1}\mu\frac{\ell^2}{2}\nabla^2u_3\nabla^2u_3\upsilon_n ds \\
& +\frac{d}{dt}\int_{R}\frac{\mu}{2}\left(\vec{\nabla}u_3\cdot\vec{\nabla}u_3\right)da+\int_{S_1}-\frac{\mu}{2}\left(\vec{\nabla}u_3\cdot\vec{\nabla}u_3\right)u_n ds+\int_{S_1}-\mu\frac{\ell^2}{2}\left(\nabla^2\dot{u}_3\vec{\nabla}u_3\right)\cdot\vec{n}ds \\
& +\frac{d}{dt}\int_{R}\frac{\mu}{2}\frac{\ell^2}{2}\nabla^2u_3\nabla^2u_3 da+\int_{S_1}-\frac{\mu}{2}\frac{\ell^2}{2}\nabla^2u_3\nabla^2u_3u_n ds \\
& +\frac{d}{dt}\int_{R}-\frac{1}{2}\rho\,\dot{u}_3\,\dot{u}_3\,d\alpha+\int_{S_1}\frac{1}{2}\rho\,\dot{u}_3\,\dot{u}_3\,\upsilon_n\,ds \\
& +\int_{S_1}\frac{\rho H^2}{12}\left(\vec{\nabla}\ddot{u}_3\dot{u}_3\right)\cdot\vec{n}ds+\int_{S_1}\frac{\rho H^2}{12}\left(\vec{\nabla}\dot{u}_3\ddot{u}_3\right)\cdot\vec{n}ds+\frac{d}{dt}\int_{R}-\frac{\rho H^2}{12}\vec{\nabla}\dot{u}_3\cdot\vec{\nabla}\dot{u}_3 d\alpha \\
& +\int_{S_1}-\frac{\rho H^2}{12}\vec{\nabla}\cdot\left(\vec{\nabla}\dot{u}_3\dot{u}_3\right)\upsilon_n ds+\int_{S_1}\frac{\rho H^2}{12}\left(\vec{\nabla}\dot{u}_3\cdot\vec{\nabla}\dot{u}_3\right)\upsilon_n ds \\
& +\int_{S_1}-\frac{\rho H^2}{12}\left(\vec{\nabla}\dot{u}_3\ddot{u}_3\right)\cdot\vec{n}ds+\frac{d}{dt}\int_{R}\frac{1}{2}\frac{\rho H^2}{12}\left(\vec{\nabla}\dot{u}_3\cdot\vec{\nabla}\dot{u}_3\right)d\alpha+\int_{S_1}-\frac{1}{2}\frac{\rho H^2}{12}\left(\vec{\nabla}\dot{u}_3\cdot\vec{\nabla}\dot{u}_3\right)u_n ds
\end{aligned}
\tag{B.4}
$$

In equation (B.4) we define the rate of a positive "potential energy" and the rate of a positive "kinetic energy";

$$
\dot{W}(t)=\frac{d}{dt}\int_{R}\frac{1}{2}\left(\mu\nabla u_3\cdot\nabla u_3+\frac{\mu\ell^2}{2}\nabla^2u_3\nabla^2u_3\right)da \tag{B.5}
$$

$$
\dot{T}(t)=\frac{d}{dt}\int_{R}\left(\frac{1}{2}\rho\dot{u}_3\dot{u}_3+\frac{1}{2}\frac{\rho H^2}{12}\nabla\dot{u}_3\cdot\nabla\dot{u}_3\right)da \tag{B.6}
$$

And thus:

$$
I=\mathscr{E}(t)-\dot{W}-\dot{T} \tag{B.7}
$$

The energy flux through the boundary S_1, can be calculated from eq. (B.4) utilizing eqs. (B.5) and (B.6) as:

Journal of Applied Mechanics. Received January 16, 2023;
Accepted manuscript posted February 08, 2023. doi:10.1115/1.4056913

$$\mathscr{E}(t)=\int_{S_1}\left[\left(\frac{\mu}{2}\vec{\nabla}u_3\cdot\vec{\nabla}u_3+\frac{\mu}{2}\frac{\ell^2}{2}\nabla^2u_3\nabla^2u_3\right)+\left(\frac{1}{2}\rho\dot{u}_3\dot{u}_3+\frac{1}{2}\frac{\rho H^2}{12}\vec{\nabla}\dot{u}_3\cdot\vec{\nabla}\dot{u}_3\right)\right]\upsilon_n ds$$
$$+\int_{S_1}\frac{1}{2}\left[-\mu\frac{\ell^2}{2}\nabla^2\left(\vec{\nabla}u_3\cdot\vec{\nabla}u_3\right)-\frac{\rho H^2}{12}\nabla^2\left(\dot{u}_3\dot{u}_3\right)\right]\upsilon_n ds \qquad \text{(B.8)}$$
$$+\int_{S_1}\left\{\left\{\left[\mu\vec{\nabla}u_3-\mu\frac{\ell^2}{2}\vec{\nabla}\left(\nabla^2u_3\right)\right]+\frac{\rho H^2}{12}\vec{\nabla}\ddot{u}_3\right\}\cdot\left(\dot{u}_3\vec{n}\right)+\mu\frac{\ell^2}{2}\left(\vec{\nabla}\dot{u}_3\right)\cdot\left(\nabla^2\dot{u}_3\vec{n}\right)\right\}ds$$

Since $W(t)\geq 0$ and $T(t)\geq 0$, uniqueness is ascertained, if $\mathscr{E}(t)$ is finite and positive. Note that for $\ell\to 0$ and $H\to 0$, eq. (B.8) reduces to the result of Freund and Clifton [49].

References

[1] Giannakopoulos, A. E., Knisovitis, C., Charalambopoulos, A., Zisis, T., and Rosakis, A. J., 2023, “Hyperbolicity, Mach Lines and Super-Shear Mode III Steady State Fracture in Magneto-Flexoelectric Materials: I. Methodology (Submitted for Publication).”

[2] Maranganti, R., and Sharma, P., 2009, “Atomistic Determination of Flexoelectric Properties of Crystalline Dielectrics,” Phys Rev B, **80**(5), p. 054109.

[3] Giannakopoulos, A. E., and Zisis, T., 2019, “Uniformly Moving Screw Dislocation in Flexoelectric Materials,” European Journal of Mechanics - A/Solids, **78**, p. 103843.

[4] Maranganti, R., Sharma, N. D., and Sharma, P., 2006, “Electromechanical Coupling in Nonpiezoelectric Materials Due to Nanoscale Nonlocal Size Effects: Green’s Function Solutions and Embedded Inclusions,” Phys Rev B, **74**(1), p. 014110.

[5] Yu, H., and Yang, W., 1994, “Mechanics of Transonic Debonding of a Bimaterial Interface: The Anti-Plane Shear Case,” J Mech Phys Solids, **42**(11), pp. 1789–1802.

[6] Huang, Y., Liu, C., and Rosakis, A. J., 1996, “Transonic Crack Growth along a Bimaterial Interface: An Investigation of the Asymptotic Structure of near-Tip Fields,” Int J Solids Struct, **33**(18), pp. 2625–2645.

[7] Guozden, T. M., and Jagla, E. A., 2005, “Supersonic Crack Propagation in a Class of Lattice Models of Mode III Brittle Fracture,” Phys Rev Lett, **95**(22), p. 224302.

[8] Koizumi, H., Kirchner, H. O. K., and Suzuki, T., 2007, “Supersonic Crack Motion in a Harmonic Lattice,” Philos Mag Lett, **87**(8), pp. 589–593.

Journal of Applied Mechanics. Received January 16, 2023;
Accepted manuscript posted February 08, 2023. doi:10.1115/1.4056913

[9] Koizumi, H., Kirchner, H. O. K., and Suzuki, T., 2007, "Lattice Wave Emission from Moving Cracks," Philosophical Magazine, **87**(27), pp. 4093–4107.

[10] Freund, L. B., 1979, "The Mechanics of Dynamic Shear Crack Propagation," J Geophys Res, **84**(B5), p. 2199.

[11] Freund, L. B., 1972, "Energy Flux into the Tip of an Extending Crack in an Elastic Solid," J Elast, **2**(4), pp. 341–349.

[12] Eshelby, J. D., 1969, "The Elastic Field of a Crack Extending Non-Uniformly under General Anti-Plane Loading," J Mech Phys Solids, **17**(3), pp. 177–199.

[13] Giannakopoulos, A. E., and Zisis, T., 2021, "Steady-State Antiplane Crack Considering the Flexoelectrics Effect: Surface Waves and Flexoelectric Metamaterials," Archive of Applied Mechanics, **91**(2), pp. 713–738.

[14] Knowles, J. K., 1966, "A Note on Elastic Surface Waves," J Geophys Res, **71**(22), pp. 5480–5481.

[15] Giannakopoulos, A. E., and Rosakis, A. J., 2022, "Dynamic Magneto-Flexoelectricity and Seismo-Electromagnetic Phenomena: Connecting Mechanical Response to Electromagnetic Signatures," J Mech Phys Solids, **168**, p. 105058.

[16] Giannakopoulos, A. E., and Zisis, T., 2021, "Uniformly Moving Antiplane Crack in Flexoelectric Materials," European Journal of Mechanics - A/Solids, **85**, p. 104136.

[17] Giannakopoulos, A. E., and Rosakis, A. J., 2020, "Dynamics of Flexoelectric Materials: Subsonic, Intersonic, and Supersonic Ruptures and Mach Cone Formation," J Appl Mech, **87**(6), p. 061004.

[18] Zhang, L., Huang, Y., Chen, J. Y., and Hwang, K. C., 1998, "The Mode III Full-Field Solution in Elastic Materials with Strain Gradient Effects," Int J Fract, **92**(4), pp. 325–348.

[19] Georgiadis, H. G., 2003, "The Mode III Crack Problem in Microstructured Solids Governed by Dipolar Gradient Elasticity: Static and Dynamic Analysis," J Appl Mech, **70**(4), pp. 517–530.

[20] Gourgiotis, P. A., and Georgiadis, H. G., 2007, "Distributed Dislocation Approach for Cracks in Couple-Stress Elasticity: Shear Modes," Int J Fract, **147**(1–4), pp. 83–102.

[21] Radi, E., 2008, "On the Effects of Characteristic Lengths in Bending and Torsion on Mode III Crack in Couple Stress Elasticity," Int J Solids Struct, **45**(10), pp. 3033–3058.

[22] Tian, X., Xu, M., Zhou, H., Deng, Q., Li, Q., Sladek, J., and Sladek, V., 2022, "Analytical Studies on Mode III Fracture in Flexoelectric Solids," J Appl Mech, **89**(4), p. 41006.

Journal of Applied Mechanics. Received January 16, 2023;
Accepted manuscript posted February 08, 2023. doi:10.1115/1.4056913

[23] Mindlin, R. D., 1968, "Polarization Gradient in Elastic Dielectrics," Int J Solids Struct, **4**(6), pp. 637–642.

[24] Gourgiotis, P. A., and Bigoni, D., 2016, "Stress Channelling in Extreme Couple-Stress Materials Part I: Strong Ellipticity, Wave Propagation, Ellipticity, and Discontinuity Relations," J Mech Phys Solids, **88**, pp. 150–168.

[25] McClintock, F., and Sukhatme, S. P., 1960, "Travelling Cracks in Elastic Materials under Longitudinal Shear," J Mech Phys Solids, **8**(3), pp. 187–193.

[26] Rubino, V., Rosakis, A. J., and Lapusta, N., 2019, "Full-Field Ultrahigh-Speed Quantification of Dynamic Shear Ruptures Using Digital Image Correlation," Exp Mech, **59**(5), pp. 551–582.

[27] Fossum, A. F., and Freund, L. B., 1975, "Nonuniformly Moving Shear Crack Model of a Shallow Focus Earthquake Mechanism," J Geophys Res, **80**(23), pp. 3343–3347.

[28] Williams, M. L., 1961, "The Bending Stress Distribution at the Base of a Stationary Crack," J Appl Mech, **28**(1), pp. 78–82.

[29] ABAQUS, 2012, *User Manual*, Hibbit, H. D., Karlsson, B. I., Sorensen, E. P.

[30] Samudrala, O., Huang, Y., and Rosakis, A. J., 2002, "Subsonic and Intersonic Shear Rupture of Weak Planes with a Velocity Weakening Cohesive Zone," J Geophys Res, **107**(B8), p. 2170.

[31] Samudrala, O., Huang, Y., and Rosakis, A. J., 2002, "Subsonic and Intersonic Mode II Crack Propagation with a Rate-Dependent Cohesive Zone," J Mech Phys Solids, **50**(6), pp. 1231–1268.

[32] Rubino, V., Rosakis, A. J., and Lapusta, N., 2020, "Spatiotemporal Properties of Sub-Rayleigh and Supershear Ruptures Inferred From Full-Field Dynamic Imaging of Laboratory Experiments," J Geophys Res Solid Earth, **125**(2), pp. 1–25.

[33] Andrews, D. J., 1976, "Rupture Propagation with Finite Stress in Antiplane Strain," J Geophys Res, **81**(20), pp. 3575–3582.

[34] Burridge, R., Conn, G., and Freund, L. B., 1979, "The Stability of a Rapid Mode II Shear Crack with Finite Cohesive Traction," J Geophys Res, **84**(B5), p. 2210.

[35] Ampuero, J. P., Vilotte, J. P., and Sánchez-Sesma, F. J., 2002, "Nucleation of Rupture under Slip Dependent Friction Law: Simple Models of Fault Zone," J Geophys Res Solid Earth, **107**(B12), p. ESE 2–1-ESE 2–19.

[36] Dunham, E. M., 2007, "Conditions Governing the Occurrence of Supershear Ruptures under Slip-Weakening Friction," J Geophys Res, **112**(B7), p. B07302.

[37] Burridge, R., 1973, "Admissible Speeds for Plane-Strain Self-Similar Shear Cracks with Friction but Lacking Cohesion," Geophys J Int, **35**(4), pp. 439–455.

Journal of Applied Mechanics. Received January 16, 2023;
Accepted manuscript posted February 08, 2023. doi:10.1115/1.4056913

[38] Mello, M., Bhat, H. S., and Rosakis, A. J., 2016, “Spatiotemporal Properties of Sub-Rayleigh and Supershear Rupture Velocity Fields: Theory and Experiments,” J Mech Phys Solids, **93**, pp. 153–181.

[39] Uenishi, K., and Rice, J. R., 2003, “Universal Nucleation Length for Slip-Weakening Rupture Instability under Nonuniform Fault Loading,” J Geophys Res Solid Earth, **108**(B1), p. ESE 17–1-ESE 17–14.

[40] Lu, X., Lapusta, N., and Rosakis, A. J., 2009, “Analysis of Supershear Transition Regimes in Rupture Experiments: The Effect of Nucleation Conditions and Friction Parameters,” Geophys J Int, **177**(2), pp. 717–732.

[41] Broberg, K. B., 1994, “Intersonic Bilateral Slip,” Geophys J Int, **119**(3), pp. 706–714.

[42] Broberg, K. B., 1996, “How Fast Can a Crack Go?,” Materials Science, **32**(1), pp. 80–86.

[43] Rosakis, A. J., 2002, “Intersonic Shear Cracks and Fault Ruptures,” Adv Phys, **51**(4), pp. 1189–1257.

[44] Freund, L. B., 1990, *Dynamic Fracture Mechanics*, Cambridge University Press.

[45] Knowles, J. K., and Pucik, T. A., 1973, “Uniqueness for Plane Crack Problems in Linear Elastostatics,” J Elast, **3**(3), pp. 155–160.

[46] Achenbach, J. D., 1793, *Wave Propagation in Elastic Solids, Applied Mathematics and Mechanics Series*, North-Holland Publishing Company.

[47] Wheeler, L. T., and Sternberg, E., 1968, “Corrigendum to the Paper ‘Some Theorems in Classical Elastodynamics,’” Arch Ration Mech Anal, **31**(5), pp. 402–402.

[48] Grentzelou, C. G., and Georgiadis, H. G., 2005, “Uniqueness for Plane Crack Problems in Dipolar Gradient Elasticity and in Couple-Stress Elasticity,” Int J Solids Struct, **42**(24–25), pp. 6226–6244.

[49] Freund, L. B., and Clifton, R. J., 1974, “On the Uniqueness of Plane Elastodynamic Solutions for Running Cracks,” J Elast, **4**(4), pp. 293–299.